UNIVERSITI MALAYA (UM)

FACULTY OF ARTS AND SOCIAL SCIENCES

DEPARTMENT OF GEOGRAPHY

SPATIOTEMPORAL EVOLUTION OF EXTREME HEAT EVENTS AND THEIR SOCIOECONOMIC CORRELATIONS IN THE YANGTZE RIVER DELTA (2000–2024)

A thesis submitted in partial fulfilment of the requirements
for the degree of Bachelor of Arts (Honours) in Geography

LIU YIXIAN

Matric Number: 23061733

Supervised by: Dr. Sheeba

May 2026

DECLARATION

I, LIU YIXIAN (Matric Number: 23061733), hereby declare that this thesis is my own original work and has not been submitted, either in whole or in part, for any other degree at this or any other institution. I confirm that all sources used in this work have been properly acknowledged and cited according to APA 7th edition referencing standards.

Signature: _____

Date: _____

LIU YIXIAN

Matric Number: 23061733

ACKNOWLEDGEMENT

I would like to express my deepest gratitude to my supervisor, Associate Professor Dr. Sheeba Nettukandy Chenoli of the Department of Geography, Universiti Malaya, whose expertise in climatology and meteorology has shaped this thesis from its first conception to its final form. Her willingness to engage critically with each draft, and to push me toward methodological rigour even when the easier path was available, is something I will carry into any future research I undertake.

I am also grateful to the Department of Geography and the Faculty of Arts and Social Sciences, Universiti Malaya, for the academic environment and the computing and GIS resources that made the spatial interpolation analyses in Chapter 4 possible. The staff and faculty members whose teaching across three years prepared me to undertake this project deserve more recognition than a single paragraph can convey.

I acknowledge the National Meteorological Information Center of the China Meteorological Administration for the station-level meteorological observations that form the empirical basis of this study, and the National Bureau of Statistics of China, together with the provincial statistical bureaux of Shanghai, Jiangsu, Zhejiang, and Anhui, for the city-level socioeconomic data used throughout. Without these publicly available datasets, the 26-city panel analysis at the heart of this thesis would not have been possible.

Finally, I thank my family for their unwavering support throughout my undergraduate studies.

Any errors that remain in this work are mine alone.

LIU YIXIAN

Kuala Lumpur, May 2026

Abstract

This thesis analyses the spatiotemporal evolution of extreme heat events across the 26 cities of the Yangtze River Delta (YRD) urban agglomeration from 2000 to 2024, and examines the relationship between heat day frequency and three socioeconomic indicators of urban development. Using monthly station observations from the China Meteorological Administration, complemented by city-level statistical yearbook data for per capita GDP, permanent resident population, and built-up area, I apply the Mann-Kendall test, Sen's slope estimator, sequential Mann-Kendall mutation point detection, inverse distance weighting interpolation, and both cross-sectional and panel first-difference Spearman correlation. The regional Sen's slope for annual heat day frequency is 0.321 days per year (MK $Z = 4.906$, $p < 0.001$), with a structural break near 2010–2011 separating a Phase I mean of 22.7 days from a Phase II mean of 27.5 days. Twelve of 26 cities show statistically significant upward trends in heat day frequency, with the steepest accumulation in inland cities (Jinhua, Sen's $\beta = 0.588$ days yr^{-1}; Chuzhou, $\beta = 0.531$). The spatial structure of heat exposure is inverted relative to economic geography: inland Anhui and western Zhejiang cities record the highest heat day counts, while the coastal core (Shanghai, Ningbo, Yancheng) records substantially lower counts, a pattern stable across all four snapshot years. Cross-sectional Spearman correlations between heat day frequency and the three socioeconomic indicators are uniformly negative and statistically significant ($\rho = -0.572$ for built-up area, -0.520 for population, -0.585 for GDP per capita), but panel first-difference correlations across the same data are near zero and non-significant. I argue that the cross-sectional result is dominated by a geographic confound between coastal position and economic development, and that the most generalisable contribution of this thesis is methodological: regional comparative studies of heat–urbanisation relationships across coastal–inland gradients are vulnerable to this confound and require either explicit geographic controls or panel-based designs to recover the underlying causal structure. The findings reallocate adaptation-planning attention from the coastal megacity core toward inland secondary cities whose heat exposure has been undercounted in the existing literature.

Keywords: extreme heat, Yangtze River Delta, urban heat island, Mann-Kendall test, Sen's slope, Spearman correlation, geographic confound, climate adaptation

Table of Contents

List of Figures

List of Tables

Chapter 1: Introduction

1.1 Background of the Study

The Yangtze River Delta (YRD) is among the most economically developed and densely settled urban agglomerations in the world, and across the 25-year window of this study it has also been the site of two transformations that interact in ways the existing literature has not fully resolved. The first transformation is climatic. Surface temperatures in eastern China have risen over recent decades at rates among the steepest documented globally for densely populated coastal regions (Zheng et al., 2021), and extreme heat events, operationally defined by the China Meteorological Administration (CMA, 2017) as days on which the daily maximum temperature meets or exceeds 35 °C, have become more frequent. The second transformation is built. The State Council's 2016 designation of 26 core cities under the Yangtze River Delta Urban Agglomeration Development Plan formalised what was already occurring on the ground: the consolidation of a continuously urbanised zone running from Shanghai westward into Anhui and southward into Zhejiang, with built-up area expanding by a factor of two to four across most of the 26 cities over the period from 2000 to the present.

Whether and how these two transformations are coupled at the city scale, and what their joint trajectory implies for heat-adaptation planning, is the question that motivates this thesis. The coupling is theoretically expected. The Urban Heat Island (UHI) literature, formalised by Oke (1982) and validated globally by Peng et al. (2012), establishes that urban surfaces modify the surface energy balance in ways that elevate near-surface temperatures relative to surrounding rural land. As cities physically grow and merge, as the YRD's coastal core has done over the past quarter-century, the relevant unit of thermal analysis shifts from the individual city to the agglomeration. The question is no longer "how much warmer is downtown than the suburbs" but "how is heat redistributed across a coalescing metropolitan region."

Three socioeconomic dimensions are usually invoked to explain the urban contribution to extreme heat. Per capita regional GDP indexes the concentration of energy-intensive activity that produces anthropogenic heat and drives demand for impervious infrastructure. Permanent resident population scales the exposure of people to whatever heat the environment delivers, and it shapes the density and form

of urban settlement. Built-up area is the most direct physical proxy for the surface modification mechanism: replacing vegetated or water-covered land with impervious cover removes the latent heat pathway and raises sensible heat flux during summer afternoons (Hao et al., 2018). The literature reviewed in Chapter 2 provides theoretical and empirical grounds for expecting each of these three dimensions to co-vary with heat day frequency. What it does not resolve is which dimension, if any, dominates at the inter-city scale over a quarter-century window in a region like the YRD.

There is a further complication that any analysis of YRD heat must confront. The dominant atmospheric driver of summer heat in eastern China is the Western Pacific Subtropical High (WPSH), whose interannual variability produces pronounced swings in heat day frequency around any longer-term trend (Ding et al., 2010). Separating the urbanisation-driven signal from the WPSH-driven variability, and both from the background warming forcing identified in the IPCC AR6 (Zhou & Qian, 2021), is methodologically demanding. Station-based observational analysis, the approach I adopt in this thesis, cannot decompose these contributions cleanly. What it can do, and what I argue is its specific contribution, is establish the empirical trajectory of heat exposure across the YRD's 26 cities and identify where the geographic pattern of that trajectory most departs from what the urbanisation-centric literature would predict.

The 2000–2024 window matters for two reasons. First, it is the period over which both the climatic and the built transformations identified above have been most rapid. Earlier decades show some warming and some urban growth, but neither at the rates documented for the post-2000 period. Second, it is the period for which CMA station data, ERA5-Land reanalysis, and the National Bureau of Statistics socioeconomic series are simultaneously available at the city level. The 24-year overlap (2000–2023) of meteorological and socioeconomic records, used in the correlation analyses reported in Chapter 4, is the longest window for which a balanced panel can be constructed for all 26 YRD cities.

1.2 Problem Statement

Three specific gaps in the existing literature motivate this thesis, each of which I address through the methodology described in Chapter 3 and the analyses reported in Chapter 4.

First, no published study has examined all 26 cities designated under the 2016 State Council Urban Agglomeration plan as a unified analytical unit across the full 2000–2024 period, using station-observed heat day counts rather than satellite-derived land surface temperature. Several recent studies treat subsets of the 26 cities (typically the coastal core), other studies use the broader Yangtze basin without restricting to the State Council boundary, and most adopt remote-sensing measures of surface skin temperature rather than the daily Tmax record that defines the CMA operational heat day threshold. The combination of unit (26-city State Council boundary), variable (station-observed heat days), and window (2000–2024) used in this study has not, to the best of my reading of the literature, been previously assembled.

Second, the spatial evolution of heat burden across the YRD's coastal–inland gradient has not been tracked through systematic multi-snapshot interpolated mapping over the post-2010 phase that the present analysis (Chapter 4) identifies as a structural break in the regional warming trajectory. Existing spatial analyses tend to focus on a single year or a single multi-year average. The four-snapshot design I use in Chapter 4 (2000, 2008, 2016, 2024) is intended to capture both the pre-mutation baseline and the post-mutation intensification, allowing comparison of spatial fields rather than single static distributions.

Third, the empirical question of which socioeconomic indicator most strongly co-varies with heat day frequency at the inter-city scale has not been resolved for the YRD over the 2000–2024 window using a panel-aware design. The theoretical literature reviewed in Chapter 2 offers competing predictions: Huang and Lu (2015) emphasise economic output, Li et al. (2024) point to built-up area, and Klein and Anderegg (2021) highlight population concentration as the dominant exposure amplifier. Resolving these competing predictions empirically requires a dataset that holds all three indicators simultaneously across comparable cities over a consistent

time period, and an analytical design that distinguishes cross-sectional from within-city associations. This thesis assembles such a dataset and applies both designs.

The three gaps share a common feature. Each constrains the empirical foundation on which heat-adaptation planning for the YRD must rest, and each is addressable with the data and methods available to a station-based comparative study. The four findings reported in Chapter 4, summarised in Chapter 5, address each of the three gaps directly.

1.3 Research Questions

Three research questions structure this thesis:

RQ1. What are the temporal trends and spatial distribution patterns of mean annual temperature and annual heat day frequency across the 26 YRD cities from 2000 to 2024, and at what point in the period did the regional trend structure undergo a detectable structural change?

RQ2. How do city-level trend magnitudes for heat day frequency vary across the inland–coastal urbanisation gradient of the YRD, and which cities have accumulated heat days most rapidly over the study period?

RQ3. What is the direction and magnitude of the Spearman rank correlation between city-level mean heat day frequency and each of three socioeconomic indicators (per capita regional GDP, permanent resident population, and built-up area of municipal districts), and how does this cross-sectional correlation compare with the within-city association observed in a panel first-difference design?

The three questions are sequential rather than parallel. RQ1 establishes the baseline temporal signal at the regional level. RQ2 disaggregates that signal to the city level, allowing identification of which portions of the urbanisation gradient have warmed most rapidly. RQ3 then asks whether the city-level variation identified in RQ2 systematically co-varies with measures of urban development. The third question is the one with the most extensive prior literature behind it, and as I show in Chapter 5, the answer is not the one the urbanisation-centric literature would predict.

1.4 Research Objectives

The research questions map to three research objectives, each of which corresponds to one analytical stream developed in Chapter 3 and reported in Chapter 4.

RO1. To quantify the regional and city-level temporal trends in annual heat day frequency and mean annual temperature across 26 YRD cities from 2000 to 2024 using the Mann-Kendall test and Sen's slope estimator, and to identify the mutation point at which the regional trend structure shifted using the sequential Mann-Kendall procedure (Sneyers, 1990).

RO2. To map the spatial redistribution of extreme heat burden across four representative years (2000, 2008, 2016, 2024) using inverse distance weighting interpolation, and to characterise the inland–coastal gradient in heat day accumulation rates and absolute heat day levels.

RO3. To assess the statistical association between city-mean annual heat day frequency and each of three socioeconomic development indicators using Spearman rank correlation, and to interpret the relationship between the cross-sectional association and within-city panel association in light of the coastal–inland geographic confound the YRD presents.

The mapping between RQs and ROs is one-to-one. The mapping between ROs and chapters is direct: §3.4 of Chapter 3 develops the methods for RO1, §3.5 for RO2, and §3.6 for RO3; correspondingly, §4.1 and §4.3 of Chapter 4 report results for RO1, §4.2 for RO2, and §4.4 for RO3.

1.5 Scope of Study

Geographically, this study covers the 26 core cities of the YRD as delimited by the 2016 State Council Yangtze River Delta Urban Agglomeration Development Plan, spanning approximately 117 °E to 123 °E longitude and 29 °N to 33 °N latitude across one direct-administered municipality (Shanghai) and three provinces (Jiangsu, Zhejiang, Anhui). The full list of 26 cities and their administrative classification appears in Chapter 3, §3.1. The boundary is the one Chinese national planning uses for the YRD; it is not the broader Yangtze basin and it is not a smaller metropolitan zone such as the Shanghai–Suzhou corridor. The choice of this specific boundary is

analytical as much as administrative: the 26 cities together span a continuous urbanisation gradient from the saturated coastal core to secondary cities in eastern Anhui that were still in early industrial expansion at the start of the study window. This gradient is what allows the comparative design that RQ2 and RQ3 rely on.

Temporally, the meteorological analysis spans the 25 years from 2000 to 2024. The socioeconomic correlation analysis uses the 2000–2023 overlap window for which both meteorological and statistical records are complete, giving 24 annual observations per city.

The primary climatic variable is annual heat day frequency, defined operationally as the count of days per calendar year on which the daily maximum temperature at the city's national-standard surface observation station meets or exceeds 35 °C. This is the CMA operational definition, and I retain it because consistency with operational thresholds matters for the policy claims I advance in Chapter 5. The secondary climatic variable is annual mean temperature, computed as the calendar-year mean of daily mean temperatures at the same station. Both variables are aggregated from the monthly time series provided by the National Meteorological Information Center.

The three socioeconomic variables are per capita regional GDP in nominal yuan, permanent resident population in units of 10,000 persons, and built-up area of municipal districts in km². The full data sourcing and homogeneity checking procedures are described in Chapter 3, §3.2.

Trend detection uses the nonparametric Mann-Kendall test (Mann, 1945; Kendall, 1975) and Sen's slope estimator (Sen, 1968) at the $\alpha = 0.05$ significance threshold. Mutation point detection uses the sequential Mann-Kendall procedure (Sneyers, 1990). Spatial interpolation uses inverse distance weighting (Shepard, 1968) with a power parameter of $p = 2$, selected by leave-one-out cross-validation. Socioeconomic correlation uses Spearman's rank coefficient (Spearman, 1904), supplemented by a panel first-difference correlation that I argue in Chapter 5 is the methodological pivot of the thesis.

This thesis does not undertake reanalysis-based atmospheric circulation diagnosis, satellite-based land surface temperature analysis, regional climate modelling, or health outcome linkage. Each of these would be a valuable extension

and is identified in Chapter 5 (§5.7) as a future research direction. The scope here is deliberately bounded to what station-based observational analysis can establish, and to the methodological lessons that follow from doing such an analysis carefully across a region with a strong coastal–inland gradient.

1.6 Significance of the Study

The significance of this thesis operates on three levels: empirical, methodological, and practical.

Empirically, the thesis contributes the most temporally extended and spatially complete city-level analysis of station-observed heat day frequency in the YRD to date. The combination of the 26-city State Council boundary, the 2000–2024 window, the station-observed heat day variable, and the city-level socioeconomic panel is, to my reading, unprecedented in the YRD literature. The four headline findings reported in Chapter 4 (regional Sen's slope of 0.321 days yr^{-1}, structural break near 2010–2011, persistent inland–coastal spatial structure, and negative cross-sectional Spearman correlations driven by geographic confounding) collectively constitute the empirical baseline against which future YRD heat-exposure assessments can be compared.

Methodologically, the thesis demonstrates a distinction whose practical importance has been underappreciated in regional heat studies. The cross-sectional Spearman correlation between heat day frequency and any of the three socioeconomic indicators across the 26 YRD cities is negative and statistically significant. The panel first-difference correlation across the same data is near zero and statistically non-significant. The two designs yield qualitatively opposite-looking conclusions about the same underlying relationship, and the resolution lies in the geographic confound the cross-sectional design cannot remove. I argue in Chapter 5 (§5.4) that this is the most generalisable contribution of the thesis: any regional comparative study of urbanisation and heat across a coastal–inland gradient is vulnerable to the same confound, and the corrective is structural rather than statistical. This argument extends beyond the YRD to comparable megaregions worldwide.

Practically, the identification of the inland Anhui corridor (Chuzhou, Anqing, Xuancheng) and inland Zhejiang (Jinhua, Huzhou) as the cities with the highest

absolute heat day frequency and the steepest accumulation rates provides spatially targeted information for heat-adaptation planning. The cities currently receiving the most attention in YRD adaptation discourse (Shanghai, Suzhou, Hangzhou) are not the cities the data identify as most heat-exposed. This is a policy claim I advance directly in Chapter 5 (§5.5), and it carries an implicit reallocation of attention away from the coastal megacity model and toward inland secondary cities whose heat exposure has been undercounted.

The three levels are not independent. The methodological caution about cross-sectional inference (the second level) is what makes the practical reallocation (the third level) credible. Without the panel first-difference comparison, the negative cross-sectional correlations might have been read, incorrectly, as evidence that the inland Anhui cities' high heat exposure was somehow a consequence of their lower socioeconomic development. The correct reading is that their high heat exposure is a feature of their inland geography, which has nothing to do with their development trajectory, and that adaptation funding should follow exposure rather than economic profile.

1.7 Structure of the Thesis

The thesis is organised into six chapters. This section provides a brief overview of how the chapters relate, both for the reader's orientation and as a map of how the three research questions are addressed across the thesis.

Chapter 2: Literature Review develops the theoretical and empirical foundations on which the research questions rest. §2.1 traces the evolution of UHI theory from Oke's foundational work through more recent agglomeration-scale studies. §2.2 examines the atmospheric mechanisms driving summer heat in eastern China, with particular focus on the WPSH. §2.3 reviews the existing literature on heat trends in the YRD specifically, including the warming asymmetry between minimum and maximum temperatures. §2.4 surveys the literature on socioeconomic correlates of urban heat. §2.5 covers the methodological literature on nonparametric trend detection and spatial interpolation. §2.6 closes by identifying the specific gaps this thesis addresses.

Chapter 3: Data and Methodology describes the data sources, preprocessing decisions, and analytical methods used to address the research questions. §3.1 defines the study area and its regional climate context. §3.2 documents the meteorological and socioeconomic data sources, including the homogeneity verification procedure for the CMA station records. §3.3 covers preprocessing decisions, including treatment of missing values and the baseline period for anomaly calculations. §3.4 develops the Mann-Kendall and Sen's slope framework used for trend analysis. §3.5 describes the IDW interpolation procedure used for spatial mapping. §3.6 explains the Spearman rank correlation approach used for the socioeconomic analysis, including the panel first-difference supplement that becomes central to the interpretation in Chapter 5.

Chapter 4: Results reports the empirical findings in four sections, each corresponding to one of the analytical streams developed in Chapter 3. §4.1 reports the regional temporal evolution of heat day frequency and mean temperature, including the sequential Mann-Kendall mutation point analysis. §4.2 presents the four-snapshot spatial interpolation across 2000, 2008, 2016, and 2024. §4.3 develops the city-level trend analysis, with Mann-Kendall significance and Sen's slope estimates for each of the 26 cities. §4.4 reports the cross-sectional Spearman correlations alongside the panel first-difference comparison, and identifies the geographic confound that the cross-sectional design cannot resolve. §4.5 summarises the four headline findings carried forward into Chapter 5.

Chapter 5: Discussion interprets the four findings in the context of the literature reviewed in Chapter 2 and identifies the limits of what station-based analysis can establish. §5.1 places the regional warming signal in broader Chinese and global context. §5.2 considers three candidate mechanisms for the 2010–2011 structural break and acknowledges that station data alone cannot adjudicate among them. §5.3 develops the spatial paradox: inland cities record higher heat day counts than coastal cities, an inversion of what the UHI literature would predict at intra-city scale, and one I attribute to maritime advection and the differential operation of the urban dry island effect. §5.4 develops the methodological argument that I argue is the thesis's most generalisable contribution. §5.5 outlines the adaptation-planning implications. §5.6 acknowledges seven limitations of the present analysis. §5.7 identifies four directions for future research.

Chapter 6: Conclusion synthesises the contributions of the thesis, returns to the three research questions to confirm what has and has not been answered, and closes with the broader implications for heat exposure analysis in densely urbanised coastal megaregions. The chapter is brief by design: the substantive interpretation rests in Chapter 5, and the conclusion serves primarily to consolidate and to signal the relationship of the thesis to subsequent work.

I have tried throughout the thesis to maintain a structure in which each chapter forward-references the next and back-references the preceding chapter explicitly. This is partly a courtesy to the reader and partly an analytical commitment. The four findings reported in Chapter 4 are not isolated empirical objects. They are the product of the analytical choices justified in Chapter 3, which themselves respond to gaps identified in Chapter 2, and they are the input to the interpretation and policy claims advanced in Chapter 5. The cross-references in the body of each chapter, and the structural map provided in this section, are intended to make that integration visible to the reader rather than leaving it for them to reconstruct.

Chapter 2: Literature Review

Chapter 2: Literature Review

Between 2000 and 2024, the Yangtze River Delta underwent two parallel and intersecting transformations. Temperatures rose across the region's 26 core cities, extreme heat days became more frequent, and the spatial footprint of the urban built environment expanded at a pace unmatched anywhere in the world during that period. Whether and how these two processes are coupled is not a question the existing literature has resolved for this specific region, time frame, and unit of analysis. This review traces how scholars have approached urban heat, extreme temperature measurement, atmospheric dynamics, and socioeconomic drivers, with the aim of establishing where current knowledge ends and where this study begins.

1. Urban Heat Island Theory: From Principles to Urban Agglomerations

1.1 Evolution of Urban Heat Island Theory

The systematic study of urban warmth begins with Luke Howard's observations of London in the early nineteenth century. Howard (1833) documented that the city centre maintained consistently higher nocturnal temperatures than surrounding rural areas, attributing this to the density of human activity and built structures. His observations were largely descriptive, but they established the empirical basis for what would later be theorised as the urban heat island.

The formal physical framework came in 1982, when Oke articulated the energy balance mechanisms underlying urban warmth. Oke (1982) introduced the Urban Canopy Layer and the Urban Boundary Layer as distinct atmospheric zones shaped by urban geometry, and identified the height-to-width ratio of street canyons as a key structural parameter controlling how heat is trapped and released. Urban materials store shortwave radiation during the day and emit longwave radiation slowly at night, disrupting the cooling that rural surfaces experience after sunset. This "cooling rate" problem remains the theoretical core of urban climatology.

The YRD complicates the single-city model. When cities physically merge and their thermal footprints overlap, the concept of a discrete heat island per city

loses analytical precision. Peng et al. (2012), working across 419 global cities, demonstrated that surface urban heat island intensity scales with city size in a non-linear fashion, with larger and denser agglomerations sustaining higher intensity and longer persistence of elevated surface temperatures. In the YRD, where Suzhou, Wuxi, Changzhou, and Shanghai form an effectively continuous built-up zone, the relevant unit of thermal analysis has shifted from the individual city to the agglomeration. Liu et al. (2021), using nighttime light imagery to characterise the spatiotemporal heterogeneity of the YRD urban agglomeration, found that thermal clustering at the regional scale had intensified substantially over the preceding two decades. Wang et al. (2024) further showed that near-surface and surface urban heat islands in the YRD are structurally distinct in their seasonal behaviour, with near-surface UHI intensifying during nighttime in summer. These findings collectively suggest that agglomeration-scale thermal dynamics cannot be inferred simply by aggregating city-level analyses.

1.2 Defining and Measuring Extreme Heat

There is no universal definition of extreme heat. The China Meteorological Administration (CMA) defines a high-temperature day as any day on which the maximum temperature reaches or exceeds 35°C, a threshold calibrated to the physiological and agronomic significance of that temperature in the Chinese context. This study adopts that threshold because the dataset drawn from CMA records uses it as the basis for the high-temperature day count variable. I refer to these days simply as 'heat days' throughout the thesis.

The ETCCDI framework, developed through a World Meteorological Organisation expert panel, offers a complementary set of indices that capture not only absolute thresholds but also distributional shifts in temperature extremes. Alexander et al. (2006), in their global analysis of daily climate extremes, validated a suite of ETCCDI indices across heterogeneous station networks and demonstrated their ability to detect trends that mean temperature analyses obscure. Of particular relevance to the YRD are the TXx index (annual maximum of daily maximum temperature), the warm spell duration indicator (WSDI), and the tropical nights index (TR), which tracks the frequency of nights where minimum temperature remains above 25°C. Yin and Sun (2018) applied these indices to Chinese station data and found that warm extremes had intensified across most of China, with the eastern

coastal zone showing among the steepest rates of increase in hot day frequency. Zheng et al. (2021), extending this analysis to 1961–2020, confirmed that the northern subtropical zone, which encompasses the YRD, exhibited accelerating trends in both TXx and TR over the most recent two decades.

The distinction between absolute thresholds and distribution-relative indices matters for interpretation. A day that exceeds 35°C in Chuzhou may represent a less anomalous departure from local climatology than the same temperature in Zhoushan, where maritime influences ordinarily suppress extremes. This study uses the absolute threshold consistent with CMA operational definitions, which is appropriate for comparing the frequency of operationally defined heat events across cities, though it means that results should be read alongside knowledge of each city's baseline climate.

2. Atmospheric Mechanisms Driving Summer Heat in Eastern China

The dominant large-scale control on summer temperature extremes in the YRD is the Western Pacific Subtropical High (WPSH). This semi-permanent anticyclonic system migrates northward and westward during boreal summer, and when it intensifies and extends over eastern China, it produces conditions favourable to extreme heat: subsiding air warms adiabatically, cloud cover is suppressed, and near-surface wind speeds weaken, trapping longwave radiation from the heated surface (Ding et al., 2010). The anomalous summer of 2013, when multiple YRD cities recorded their highest temperatures in decades, coincided with an unusually persistent westward extension of the WPSH.

Ding et al. (2010), analysing changes in hot days and heatwaves across China from 1961 to 2007, found that WPSH variability explained a substantial fraction of interannual variance in heat day frequency across the Yangtze basin, but that the long-term trend could not be attributed to WPSH behaviour alone. Urbanisation, they noted, amplified the WPSH-driven heat signal in cities through changes to surface albedo, evapotranspiration, and anthropogenic heat release.

The interaction between large-scale atmospheric circulation and local surface modification is an active research frontier. Xie et al. (2017) used regional climate modelling to demonstrate that urbanisation-induced land cover change and increased pollutant emissions in the YRD had measurably altered the boundary layer structure,

enhancing heat accumulation during synoptically stagnant periods. Hao et al. (2018) documented the corollary of this process in the YRD: the urban dry island effect, whereby the replacement of vegetated land with impervious surfaces reduces latent heat flux and elevates sensible heat flux, increasing surface and near-surface temperatures while reducing atmospheric humidity relative to rural surroundings.

What this means for interpretation is that observed trends in heat day frequency in any YRD city are products of at least three overlapping signals: the global warming background, interannual WPSH variability, and local surface modification from urbanisation. Separating these signals is methodologically demanding and beyond the scope of the current study. The Mann-Kendall approach used here tests for monotonic trends without decomposing their sources. That is a recognised limitation of station-based trend analysis (Zhou & Qian, 2021), and is acknowledged explicitly in the Discussion chapter. I return to the question of separating WPSH variability from urbanisation effects in Chapter 5.

3. Spatiotemporal Trends in the Yangtze River Delta

3.1 Documented Warming Rates and Temperature Asymmetry

The most detailed city-level analysis of warming in the YRD remains Huang and Lu (2015), who examined 23 cities within the agglomeration and found that the UHI effect contributed a warming rate beyond the regional background signal. Large cities in the YRD warmed at approximately 0.483°C per decade, while smaller peripheral cities warmed at around 0.179°C per decade over the same period. The differential, they argued, was attributable primarily to urban growth rather than to spatial variation in large-scale climate forcing, given that the regional background warming signal is relatively uniform at this spatial scale. This is the most widely cited quantitative benchmark for UHI-attributable warming in the YRD and informs the analytical expectations of the present study.

One consistent finding in the broader Chinese temperature record is that minimum temperatures are rising faster than maximum temperatures. Zheng et al. (2021) confirmed this asymmetry across multiple temperature zones in China, finding that warm night indices increased more steeply than warm day indices in the northern subtropical zone. Nights that remain above 25°C prevent physiological recovery and compound health risk over multi-day heatwave sequences. This

asymmetry is not captured by the heat day count used in the current study, which counts days with maximum temperature meeting or exceeding 35°C — a limitation worth acknowledging when interpreting results.

3.2 Spatial Distribution and Its Evolution

Early work on the spatial structure of YRD heat tended to focus on the coastal economic core: Shanghai, Nanjing, Hangzhou, and the Suzhou-Wuxi corridor. This was partly because those cities had denser station networks and better data coverage, and partly because the theoretical expectation was that the largest and most economically developed cities would have the most intense heat islands.

The picture that emerges from more recent literature is more spatially diffuse. Li et al. (2024), using an XGBoost-SHAP framework to decompose land surface temperature drivers across the YRD urban agglomeration, found that built-up area expansion in secondary and peripheral cities was associated with steeper marginal increases in surface temperature than equivalent expansion in the already-saturated coastal cores. Zhai et al. (2020) showed that the economic efficiency of built-up land use was negatively associated with urban heat island intensity: cities with more economically productive land use had lower heat intensification per unit area, a finding that complicates simple linear narratives linking GDP growth to heat. Liu et al. (2021) demonstrated that the nighttime light signature of economic activity had expanded substantially beyond the historical coastal core into central Zhejiang and eastern Anhui. Whether the thermal frontier had followed the same trajectory was not directly addressed by these studies and this gap is one that the current study is positioned to investigate.

4. Socioeconomic Correlates of Extreme Heat: Evidence and Debates

4.1 Economic Development and the GDP-Heat Relationship

The connection between economic growth and urban warming in China is well-established at the provincial and national scale. Huang and Lu (2015) identified a positive relationship between per capita GDP and UHI intensity in the YRD, attributing it to the concentration of energy-intensive activity and building stock in wealthier cities. Luo et al. (2022) specifically examined economic drivers of the urban heat island in the YRD and found that GDP growth was associated with

increased heat island intensity, though the relationship was not uniform across city size categories.

The STIRPAT framework, first proposed by Dietz and Rosa (1994) and extended by York et al. (2003) into a multiplicative stochastic model of environmental impact, has been applied in several Chinese urban heat studies to decompose the relative contributions of population, affluence, and technology to local warming. Studies using this framework in the YRD context have generally found affluence, measured as GDP per capita, to be a significant term, though its coefficient is smaller than that associated with built-up area expansion. The problem with STIRPAT in this context is that affluence and urbanisation are collinear in rapidly developing cities. Disentangling their independent contributions requires either instrumental variable methods or long enough time series to observe variation in their growth rates. The Spearman correlation approach used in the current study does not resolve this collinearity, and the results should be read accordingly.

4.2 Population Agglomeration and Exposure Risk

Klein and Anderegg (2021) projected that heat exposure globally would increase substantially over the twenty-first century, driven by a combination of background warming and continued urban population growth. Their analysis showed that even without additional warming beyond current commitments, the sheer concentration of people in cities that are already warm would substantially increase the number of person-days of heat exposure. In the YRD, this dynamic is already visible: Oleson et al. (2015) argued that the interaction between urbanisation and heat stress creates a non-linear exposure risk as population density rises, because denser areas have less green space, higher impervious surface fractions, and more anthropogenic heat release per unit area.

The health consequences are documented. Ebi et al. (2021), synthesising evidence from global heatwave literature, identified cardiovascular and cerebrovascular events as the primary causes of excess mortality during heat events. Zhou et al. (2022), focusing on East Asian cities, found that the burden of heat-related stroke mortality increased with both warming and urbanisation, and that older populations in dense cities were disproportionately exposed. Nanjing, Shanghai, and Hangzhou, all within the YRD, carry high proportions of elderly residents and are

expected to see greater health impacts per unit of temperature increase than cities with younger demographic profiles.

4.3 Built-Up Area Expansion and Surface Energy Modification

Of the three socioeconomic variables considered in this study, built-up area is the most proximate physical driver of heat island formation. The mechanism is direct: replacing vegetated or water-covered land with impervious surfaces removes the latent heat pathway. Energy that would otherwise drive evapotranspiration instead warms the surface and overlying air. Hao et al. (2018) quantified the resulting urban dry island effect in the YRD and showed that the magnitude of the drying effect scaled with the extent of impervious surface coverage.

Zhai et al. (2020) added spatial granularity by showing that the relationship between built-up area expansion and heat island intensity in the YRD was non-linear: heat intensification was steeper during the earlier phases of urban expansion, when high-quality evapotranspiring land was converted, and more moderate during later infill development, when expansion occurred into already-degraded peri-urban land. Li et al. (2024), using more recent data and machine learning attribution, confirmed that built-up area remained the dominant structural predictor of land surface temperature across the agglomeration, outweighing both economic output and population density as marginal explanatory variables. These findings provide the strongest literature-based rationale for expecting built-up area to produce the highest Spearman correlation coefficient in the current study's correlation analysis.

5. Methodological Approaches in Regional Heat Studies

5.1 Trend Detection

Station-based meteorological time series for Chinese cities are often non-normally distributed due to interannual climate variability, which violates the assumptions underlying ordinary least squares regression. The Mann-Kendall test, first formalised by Mann (1945) as a nonparametric test against trend, addresses this by working with ranks rather than raw values. It makes no assumption about the underlying distribution of the data and is robust to outliers. Paired with Sen's slope estimator (Sen, 1968), which uses the median of all pairwise slopes in a time series to estimate the rate of change, the MK-Sen framework has become standard in Chinese

meteorological trend studies (Zhou & Qian, 2021; Zheng et al., 2021). Cao et al. (2016) demonstrated the importance of prior homogenisation in Chinese station data before trend analysis, showing that uncorrected station relocations and instrument changes introduced spurious shifts that could be mistaken for real climate signals.

5.2 Spatial Interpolation

Meteorological stations are point observations. Generating continuous spatial fields from them requires interpolation, and the choice of method introduces its own assumptions. Inverse Distance Weighting (IDW) is among the simplest and most transparent: it assigns each unsampled location a weighted average of surrounding stations, with weights declining as a power function of distance (Shepard, 1968). In the YRD, the flat plains of the Taihu Basin and the lower Yangtze are well-suited to IDW, but the hilly southwestern portions of the study area introduce topographic complexity that IDW cannot account for. Interpolated values in these areas should be treated as approximations.

5.3 Socioeconomic Correlation Analysis

Spearman's rank correlation is appropriate when variables are not normally distributed or when the relationship is expected to be monotonic but not necessarily linear. City-level GDP per capita in the YRD is strongly right-skewed, with Shanghai's values far exceeding those of Anhui peripheral cities in the early 2000s. Pearson correlation in this context would give undue weight to outlier observations. Spearman's transformation to ranks neutralises this problem (Spearman, 1904). The coefficient measures the strength of monotonic association: whether higher values of one variable are systematically paired with higher values of another, without requiring proportionality. This is a more defensible approach for the data structure in question, though it sacrifices information about the shape of the relationship.

6. Research Gaps and the Position of This Study

The literature reviewed above has established several things with reasonable confidence. Extreme heat in the YRD has increased in both frequency and intensity since 2000. The UHI contributes to warming rates that exceed the regional background. Socioeconomic variables, particularly built-up area and population, are

positively correlated with heat intensity. Large cities in the coastal core have warmed faster than smaller peripheral cities, at least through the mid-2010s.

What remains unresolved is more specific. No published study has systematically compared all 26 cities designated under the 2016 YRD Urban Agglomeration Development Plan across the full 2000–2024 period using a common set of meteorological observations and socioeconomic indicators drawn at the city level. Available studies are either spatially limited, temporally limited, or methodologically focused on land surface temperature from satellite imagery rather than station-observed heat day frequency. The spatial evolution of extreme heat burden across the full urbanisation gradient, from the megacities of the eastern coast to the secondary cities of inland Anhui, has not been mapped in a way that tracks relative warming trajectories of individual cities over 25 years.

There is also a specific empirical question the existing literature raises but does not answer: whether the socioeconomic variable most strongly correlated with heat frequency at the city level is GDP per capita, permanent resident population, or built-up area expansion. The theoretical arguments and individual studies reviewed above point in different directions. Huang and Lu (2015) emphasise economic output; Li et al. (2024) and Zhai et al. (2020) point to built-up area as the dominant physical mechanism; Klein and Anderegg (2021) highlight population as the exposure amplifier. Resolving this empirically requires a dataset holding all three variables simultaneously across comparable cities over a consistent time period. That is what the database constructed for this study provides. Whether cross-sectional Spearman correlation can isolate the relative strength of each variable depends, however, on the degree to which socioeconomic gradients align with underlying climatic gradients across the study area. If the cities with the strongest economies are also those with the most moderate baseline climates, the cross-sectional comparison will capture geographic exposure differences rather than urbanisation effects. This possibility is evaluated directly in the Results chapter. I operationalise these three mechanisms—UHI, WPSH variability, and socioeconomic drivers—through the methods set out in Chapter 3.

Chapter 3: Data and Methodology

Chapter 3: Data and Methodology

3.1 Study Area

3.1.1 Geographic Scope and Administrative Delineation

The 26 core cities designated under the Yangtze River Delta Urban Agglomeration Development Plan, formally approved by the State Council of China in 2016, define the spatial boundary of this study. Geographically, this boundary spans approximately 117°E to 123°E longitude and 29°N to 33°N latitude, covering a total land area of approximately 211,700 square kilometres. The cities included are: Shanghai (one direct-administered municipality); Nanjing, Wuxi, Changzhou, Suzhou, Nantong, Yancheng, Yangzhou, Zhenjiang, and Taizhou in Jiangsu Province; Hangzhou, Ningbo, Jiaxing, Huzhou, Shaoxing, Jinhua, Zhoushan, and Taizhou in Zhejiang Province; and Hefei, Wuhu, Ma'anshan, Tongling, Anqing, Chuzhou, Chizhou, and Xuancheng in Anhui Province.

Terrain varies substantially across this range. The north and east are dominated by flat alluvial plains, including the Taihu Basin and the lower Yangtze floodplain. Moving southwest, the landscape gives way to increasingly hilly terrain where the Tianmu and Huangshan ranges introduce elevation-driven temperature gradients that point-based interpolation cannot fully resolve. Results for cities situated in complex topography — Jinhua, Chizhou, Xuancheng, and Taizhou (Zhejiang) — should be read with that constraint in mind.

Selecting the 2016 State Council boundary, rather than provincial or economic zone boundaries, was a deliberate analytical choice. The plan's 26-city delineation crosses three provincial administrations and captures a continuous built-up gradient from the saturated metropolitan core of the Suzhou-Shanghai corridor to secondary cities in eastern Anhui still in early phases of industrial expansion at the start of the study period. Provincial boundaries would have fractured this gradient artificially.

3.1.2 Regional Climate Context

The Yangtze River Delta falls within the northern subtropical monsoon climate zone. Winters are governed by cold, dry airflows from the Mongolian-Siberian High; summers are controlled by the Western Pacific Subtropical High (WPSH), which brings warm, moist southeasterly airflow across the region. Annual mean temperatures across the 26 cities average approximately 17–18°C, with annual precipitation of roughly 1,100–1,700 mm concentrated in the June–July plum rain season and the August–September typhoon season.

Extreme summer heat is mechanistically tied to the behaviour of the WPSH. When this system strengthens and extends westward over eastern China, the YRD lies beneath descending anticyclonic circulation. The sinking air warms adiabatically, cloud cover is suppressed, incoming shortwave radiation at the surface intensifies, and near-surface winds weaken. Heat accumulates. Ding et al. (2010), analysing hot day trends across China from 1961 to 2007, identified WPSH variability as the primary interannual control on heat day frequency across the Yangtze basin, while noting that the multi-decadal upward trend in heat day counts could not be explained by circulation variability alone — a point that motivates the urbanisation correlation analysis in this study.

3.1.3 The Urbanisation Gradient as Analytical Framework

A study covering 26 cities rather than one requires justification. The YRD is used here not merely as a geographic container but as a natural gradient experiment. Shanghai and Suzhou represent mature, high-density urban economies. Chuzhou and Xuancheng represent cities where built-up expansion recorded in statistical yearbooks was still accelerating through the 2010s. Because these cities occupy broadly similar latitudinal and climatic positions, variation in their extreme heat trajectories is more plausibly attributable to differences in urban development than to differences in background climate forcing. Huang and Lu (2015) used a comparable cross-city framework within the YRD to attribute differential warming rates to urban growth rather than spatial variation in large-scale atmospheric dynamics. This study extends that logic from mean temperature warming rates to extreme heat day frequency, and pushes the temporal horizon to 2024. I apply this gradient-design logic throughout Chapter 4.

3.2 Data Sources

3.2.1 Archived Meteorological Data

Meteorological data for this study are drawn from archived records published by the National Meteorological Information Center of the China Meteorological Administration (NMIC-CMA), accessed via the China Meteorological Data Network (data.cma.cn). Station-level monthly records were extracted for all 26 cities from January 2000 to December 2024. Two variables were extracted.

Monthly mean temperature (°C) is the arithmetic mean of daily mean temperatures recorded at the designated national-standard surface observation station for each city, aggregated to monthly values by the NMIC. Annual high-temperature day count is the number of days per year on which the daily maximum temperature at the station met or exceeded 35°C, consistent with the CMA's operational definition of a high-temperature day (China Meteorological Administration, 2017). For trend analysis, annual totals were calculated by summing monthly counts from June through September, the months within which effectively all heat days in the YRD occur.

Station homogeneity is a documented problem in long Chinese meteorological records. Relocations, instrument replacements, and protocol changes introduce step changes that can be mistaken for real climate signals. Cao et al. (2016) demonstrated that uncorrected discontinuities in the NMIC dataset are large enough to affect Mann-Kendall trend detection. To address this, monthly temperature series for each city were cross-checked against ERA5-Land reanalysis data (spatial resolution approximately 9 km) for the nearest grid cell to each station. The scale mismatch between point-based station observations and grid-cell averages means that absolute values are not directly comparable; what is compared is the temporal structure. Specifically, a step change was flagged when the month-to-month difference in station temperature exceeded 1.5 standard deviations of the city-specific monthly difference distribution, and no corresponding shift of similar timing and magnitude appeared in the ERA5-Land series for the same grid cell. Flagged values were then checked against station metadata records from NMIC for documented relocations or instrument changes. Where no documented cause was identified and the discrepancy exceeded the threshold, the affected values were treated as missing

and filled by linear interpolation between adjacent valid observations or neighbouring station records.

3.2.2 Archived Socioeconomic Data

Socioeconomic data were drawn from archived statistical yearbooks issued by the National Bureau of Statistics of China and provincial statistical bureaux (National Bureau of Statistics of China, 2024). For each of the 26 cities and each year from 2000 to 2023, three variables were extracted: per capita regional GDP in nominal yuan; permanent resident population in units of 10,000 persons; and built-up area of municipal districts in km², as reported in annual urban construction statistical yearbooks. The built-up area variable reflects the total area of continuous urban construction land within the municipal district boundary and is used here as a proxy for the cumulative physical footprint of urbanisation, which is the mechanism most directly linked to surface energy balance modification.

Socioeconomic records are available through 2023 only. The meteorological dataset extends through 2024. Correlation analyses linking heat day frequency to socioeconomic variables therefore use the 2000–2023 overlap period, giving 24 annual observations per city.

3.2.3 Variable Summary

Table 1: Core variables, units, sources, and sample coverage.

Variable	Unit	Source	Coverage	N
Monthly mean temperature	°C	NMIC-CMA	2000–2024	26 × 25 × 12
Annual high-temperature days	Days	NMIC-CMA	2000–2024	26 × 25
Per capita regional GDP	Yuan (nominal)	Provincial stat. yearbooks	2000–2023	26 × 24
Permanent resident population	10,000 persons	City stat. bulletins	2000–2023	26 × 24
Built-up area, municipal districts	km²	Urban construction yearbooks	2000–2023	26 × 24

3.3 Data Preprocessing

3.3.1 Homogeneity Verification and Missing Value Treatment

Beyond the ERA5 cross-validation described above, the socioeconomic series were screened using a 3σ criterion: observations exceeding three standard deviations from the city-specific mean for any variable were examined against the source yearbook. Several large year-on-year changes in built-up area reflected administrative boundary reclassifications rather than actual construction. These were corrected to continuity-adjusted values with a note attached to the affected city-year observations. Missing values in the meteorological series totalled fewer than 0.4% of monthly observations across all cities and years, and were filled by linear interpolation.

3.3.2 Normalisation

Per capita regional GDP in the YRD dataset is strongly right-skewed. Shanghai's values exceed those of Chizhou by a factor exceeding fifty in the early years of the study period. Since Spearman's rank correlation operates on rank order rather than raw magnitudes, this skewness does not affect the correlation coefficients directly. Normalisation using Min-Max scaling was applied only for the scatter matrix visualisation in the Results chapter, to enable visual comparison of distributions across variables with different numerical scales. It was not applied to the correlation analysis itself.

3.3.3 Climate Baseline Period

Temperature anomaly values were calculated relative to the 2000–2010 baseline period. This decade was chosen as the reference because it represents the earliest ten-year window of complete and verified data coverage across all 26 cities, predating what the mutation point analysis identifies as the structural acceleration in regional warming. For each city, the anomaly in any subsequent year is the difference between that year's annual mean temperature and the city's 2000–2010 mean.

3.4 Trend Analysis: Mann-Kendall Test and Sen's Slope Estimator

3.4.1 Mann-Kendall Test

Following the methodological consensus reviewed in §2.5, I adopt the Mann-Kendall framework rather than OLS regression. Applying ordinary least squares regression to test for trends in climate time series assumes that residuals are normally distributed and homoscedastic. Annual high-temperature day counts in the YRD frequently violate both assumptions: the distribution is bounded at zero, variance is unequal across years with different WPSH behaviour, and individual anomalous years can exert disproportionate leverage on slope estimates. The Mann-Kendall test addresses this by working with ranks rather than raw values. Originally proposed by Mann (1945) and extended for meteorological use by Kendall (1975), it tests the null hypothesis of no monotonic trend without requiring any particular distributional form.

The test statistic S is computed as:

$$S = \Sigma_{i=1 \text{ to } n-1} \Sigma_{j=i+1 \text{ to } n} \operatorname{sgn}(x_j - x_i)$$

where x_i and x_j are observed values at time points i and j, and the sign function $\operatorname{sgn}(\theta)$ returns +1 if $\theta > 0$, 0 if $\theta = 0$, and -1 if $\theta < 0$.

The variance of S, corrected for ties, is:

$$\mathrm{Var}(S) = [n(n-1)(2n+5) - \Sigma\, t_p(t_p-1)(2t_p+5)] / 18$$

where the summation is over g tied groups, and t_p is the number of observations in the p-th tied group. The standardised statistic Z follows:

$$Z = (S-1) / \sqrt{\mathrm{Var}(S)} \text{ if } S > 0; \quad Z = 0 \text{ if } S = 0; \quad Z = (S+1) / \sqrt{\mathrm{Var}(S)} \text{ if } S < 0$$

A positive Z indicates an upward trend; negative indicates downward. The null hypothesis is rejected at $\alpha = 0.05$ when $|Z| > 1.96$. The test is applied separately to each of the 26 cities for both annual mean temperature and annual high-temperature day count.

Note: The formulae above are presented in plain-text notation for document portability. In the final formatted thesis submission, these should be rendered using the Equation Editor in Microsoft Word or converted from LaTeX. The LaTeX equivalents are available from the author.

3.4.2 Sen's Slope Estimator

Knowing that a trend is statistically significant is not the same as knowing how fast the change is occurring. Sen's slope estimator (Sen, 1968) provides a magnitude estimate by computing the median of all pairwise slopes in the series:

$$\beta = \text{Median}[(x_j - x_i) / (j - i)] \quad \text{for all } j > i$$

Using the median rather than the mean makes the estimator resistant to years in which anomalously extreme values would inflate or deflate a mean-based slope. The resulting β value expresses the rate of change per year in the original units of the variable. City-level β values are compared across the 26 cities to identify which portions of the urbanisation gradient are accumulating heat days most rapidly.

3.4.3 Mutation Point Detection

The sequential Mann-Kendall procedure described by Sneyers (1990) generates two cumulative statistics from the same series: the forward statistic UF, computed in chronological order, and the backward statistic UB, computed in reverse. The intersection of UF and UB identifies the approximate timing of a possible structural shift in trend behaviour. Crucially, the reliability of this timing estimate depends on whether the intersection falls within the ±1.96 confidence bounds: intersections occurring outside the bounds indicate that the trend was already statistically established before or after the candidate breakpoint, making the exact timing less certain. When the intersection falls near the boundary itself, the mutation point should be treated as an approximate indicator rather than a precisely dated event. This procedure is applied to the regional aggregated heat day series to determine whether a discernible mutation point exists within 2000–2024. The result informs how the temporal narrative of the Results chapter is structured and what baseline period is most appropriate for anomaly calculations.

3.5 Spatial Interpolation: Inverse Distance Weighting

3.5.1 IDW Algorithm and Parameter Selection

I selected IDW with p = 2 after testing values from 1 to 4 against leave-one-out RMSE; with 26 stations across 211,700 km², kriging requires a variogram that cannot be estimated reliably. Twenty-six station observations do not constitute a spatial field. Converting them into one requires an interpolation method, and the

choice carries assumptions that need to be stated. Kriging, the geostatistical alternative to IDW, requires an empirical variogram fitted from the data and is most useful when the density of observations is sufficient to estimate spatial autocorrelation structure reliably. With 26 points distributed across 211,700 km², the variogram is poorly constrained. IDW, introduced by Shepard (1968) and later refined for heterogeneous station networks (Lu & Wong, 2008), is a more transparent and appropriate choice here: it assigns each prediction location a weighted average of surrounding station values, with weights declining as a power function of the separation distance.

The IDW formula is:

$$\hat{z}(x) = [\Sigma\, w_i(x)\, z_i] / [\Sigma\, w_i(x)], \text{ where } w_i(x) = 1 / d(x, x_i)^p$$

Here $\hat{z}(x)$ is the estimated value at prediction point x, z_i is the observed value at station x_i, $d(x, x_i)$ is the Euclidean distance between the prediction point and station i, and p controls how steeply weights decline with distance.

The power parameter was set to p = 2 following cross-validation across the 26 stations. Values of p from 1 to 4 were tested; p = 2 produced the minimum leave-one-out RMSE across both the annual mean temperature and heat day surfaces. Lower values of p produced over-smoothed surfaces that flattened the contrast between hotspot cities; higher values produced target-like bullseye artefacts centred on individual stations. All interpolation was performed in ArcGIS Pro using the CGCS2000 geodetic coordinate system, which ensures that Euclidean distance calculations reflect true ground distances across the study area.

3.5.2 Temporal Comparison Points

Interpolation was performed for four years: 2000, 2008, 2016, and 2024. These points were selected to bracket the study period and capture distinct phases of urbanisation rather than to track year-on-year variation. Annual high-temperature day totals for each city in each of the four years serve as the input values. The resulting surfaces are compared as a four-panel figure in the Results chapter. Given the limitations of IDW over complex terrain noted in Section 3.1.1, the southwestern portions of each interpolated surface should be treated as approximations rather than precise estimates.

3.6 Socioeconomic Correlation: Spearman's Rank Correlation

3.6.1 Rationale for Non-parametric Approach

I use Spearman's rank correlation rather than Pearson's because per capita GDP spans nearly two orders of magnitude across the 26 cities. Pearson's correlation coefficient measures linear association and is sensitive to the assumption that both variables are approximately normally distributed. Neither condition holds comfortably here. Per capita GDP across the 26 cities spans roughly 3,400 to 206,000 yuan over the study period, a distribution dominated by the coastal economic core and with a long right tail toward the Anhui periphery. Applying Pearson's correlation to this data structure would give undue weight to the handful of city-years at the extreme upper end of the GDP range. Spearman's rank correlation (Spearman, 1904) sidesteps this by substituting ranks for raw values before computing the association measure, so that what is tested is whether higher-ranked cities on one variable tend to be higher-ranked on the other. No assumption is made about the shape of either distribution.

3.6.2 Correlation Pairs and Analytical Structure

The Spearman coefficient r_s is computed as:

$$r_s = 1 - (6 \Sigma d_i^2) / [n(n^2 - 1)]$$

where d_i is the rank difference for observation i and n is the number of paired observations. This formula assumes no tied ranks. In practice, tied values occur when two or more cities share the same rank on a variable; the computation was performed using SciPy (version 1.11), which assigns mid-ranks to tied observations and applies a correction factor to the variance estimate, yielding accurate p-values even with ties present. Three variable pairs are computed: annual high-temperature days against built-up area; annual high-temperature days against permanent resident population; and annual high-temperature days against per capita regional GDP. Each pair uses city-level means across the 2000–2023 overlap period as the unit of analysis, giving 26 paired observations. Results are reported at two-tailed significance thresholds of $p < 0.05$, $p < 0.01$, and $p < 0.001$.

One interpretive boundary must be drawn clearly. Built-up area, population, and GDP co-vary across these 26 cities: wealthier cities tend to be larger and more

densely populated. A higher Spearman coefficient for built-up area than for GDP does not establish that land expansion is the causal mechanism and economic output is not. What the correlation comparison does establish is which socioeconomic dimension most consistently co-varies with extreme heat frequency across the gradient. Causal attribution would require either controlled experiments or regression designs that isolate individual drivers — neither of which is feasible with this dataset. That constraint is engaged directly in the Discussion. The geographic confound this method cannot resolve is taken up directly in §4.4 and discussed in Chapter 5.

Chapter 4: Results

Chapter 4: Results

The results are organised into four sections that follow the sequence of the analytical framework set out in Chapter 3. Section 4.1 documents the temporal trajectory of extreme heat events and mean temperature across the 26-city region, including the mutation point at which the trend structure shifted. Section 4.2 traces the spatial redistribution of heat burden across four temporal snapshots. Section 4.3 presents city-level trend magnitudes and their provincial patterns. Section 4.4 reports the Spearman rank correlations linking heat day frequency to the three socioeconomic indicators, and addresses the geographic confound that shapes the cross-sectional results.

Throughout, "heat days" refers exclusively to days on which daily maximum temperature met or exceeded 35°C, consistent with the China Meteorological Administration operational threshold (CMA, 2017). All trend statistics are based on 25-year annual series from 2000 to 2024; the correlation analysis uses the 2000–2023 overlap period where both meteorological and socioeconomic records are complete (n = 26 city means). Statistical significance thresholds of $p < 0.05$ (*), $p < 0.01$ (), and $p < 0.001$ (**) apply throughout.

4.1 Regional Temporal Evolution of Extreme Heat Events

4.1.1 Trend in Annual High-Temperature Days

The regional mean annual high-temperature day count, averaged across all 26 cities, increased significantly over the 2000–2024 period (Mann-Kendall $Z = 4.906$, $p < 0.001$). The Sen's slope estimate is 0.321 days per year, implying an accumulation of approximately 7.7 additional heat days over the full study period. Figure 4.1a illustrates the year-by-year series. The series is characterised by pronounced interannual variability around the upward trend: the lowest regional mean occurred in 2005 (21.0 days) and the highest in 2022 (29.3 days), a within-period range of 8.3 days.

The trajectory is not uniform across the study period. The period 2000–2010 produced a regional mean of 22.7 days per year. Over the subsequent phase, 2011–

2024, the mean rose to 27.5 days, an increase of 4.8 days (+21.0%). This shift is reflected in the sequential Mann-Kendall statistics: the forward statistic UF remained within the ±1.96 confidence bounds through 2010, indicating no statistically established trend up to that point, before crossing the threshold in 2011 (UF = 2.41) and accelerating thereafter to reach UF = 5.80 by 2024. The UF and UB series intersect at approximately 2010–2011 (Figure 4.1b), identifying this as the probable mutation point in the regional trend structure. Because the intersection occurs as UF crosses the 1.96 significance boundary, this is consistent with a pattern in which the underlying signal was present but too weak to be detected statistically until the post-2010 accumulation of anomalous years reinforced it.

Several individual years warrant brief identification. The year 2013 is widely documented as an exceptional regional heat extreme (Wang et al., 2024; Zheng et al., 2021); in this dataset, the 2013 regional mean of 26.7 days stands above the 2000–2010 baseline mean by approximately 4.0 days. The years 2022 and 2024 represent the two highest recorded regional means (29.3 and 28.7 days respectively), suggesting that the most recent phase of the record captures the most intense multi-year heat accumulation of the study period. The year 2023, by contrast, produced a regional mean of 27.2 days, lower than 2022 and consistent with the interannual variability that prevents any single year from being read as definitive evidence of monotonic acceleration. This mutation point anchors the spatial snapshots in §4.2 and the city-level analysis in §4.3.

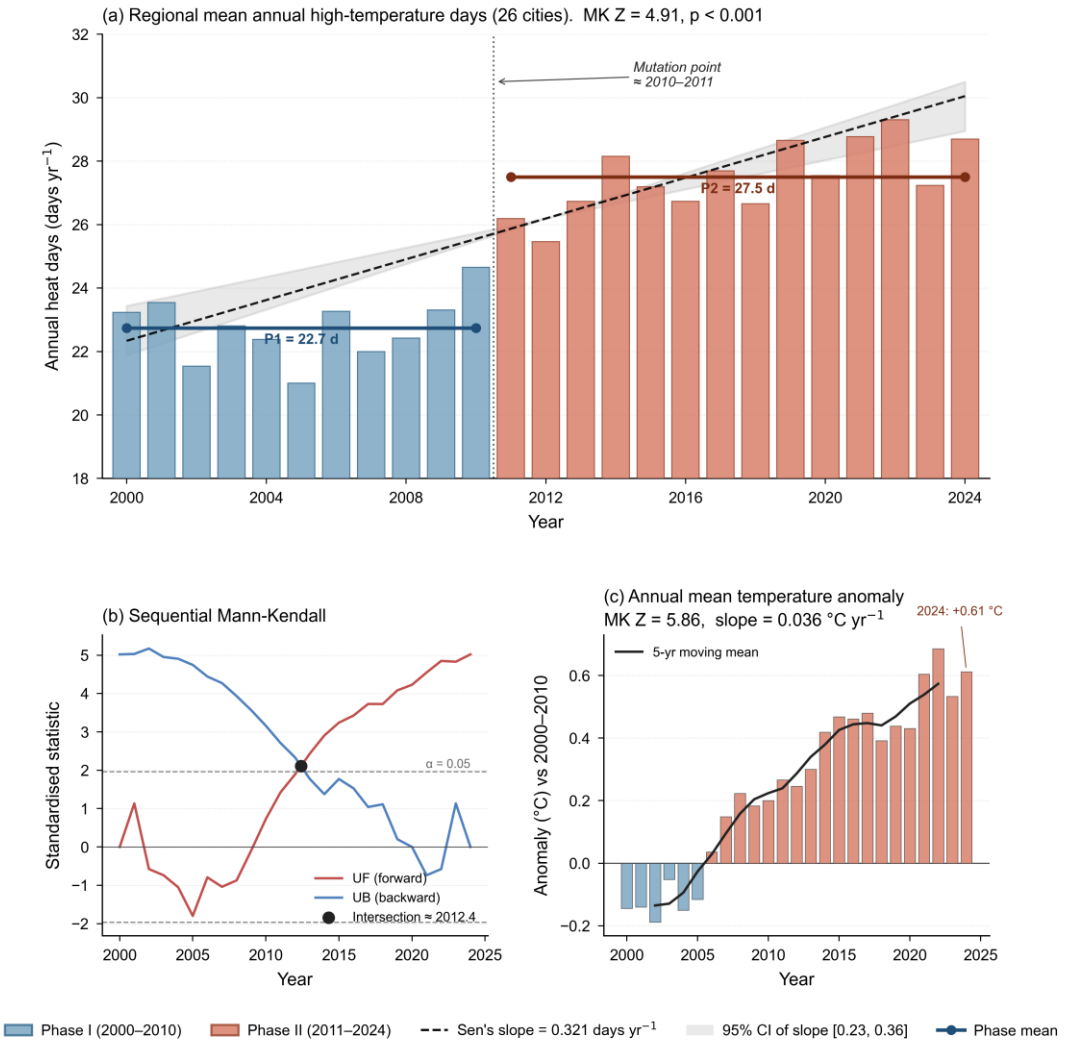

Figure 4.1. Regional temporal evolution of extreme heat events in the Yangtze River Delta, 2000–2024. (a) Annual mean heat days across 26 cities, with Sen's slope trend line (dashed), period means (horizontal bars), and two-phase shading demarcated at the 2010–2011 mutation point. (b) Sequential Mann-Kendall forward (UF) and backward (UB) statistics; intersection of UF and UB near 2010–2011 indicates the probable structural break. (c) Annual mean temperature anomaly relative to the 2000–2010 baseline, with five-year moving mean.

4.1.2 Concurrent Warming in Annual Mean Temperature

The regional mean annual temperature also exhibited a significant upward trend over the study period (Mann-Kendall Z = 5.862, p < 0.001), with a Sen's slope of 0.036°C per year. The cumulative estimated warming from 2000 to 2024 is approximately 0.85°C. Temperature anomalies calculated relative to the 2000–2010 baseline (Figure 4.1c) remained near zero through the first decade but turned consistently positive from 2011 onward. By 2022, the regional anomaly reached

+0.69°C; by 2024 it stood at +0.61°C. These values are consistent with the broader national trend reported by Zheng et al. (2021) for the northern subtropical zone.

The synchrony between the temperature anomaly series and the elevated heat day counts in Phase II (2011–2024) is consistent with a background warming signal amplifying the frequency of days exceeding the 35°C threshold. The temperature trend, however, cannot be cleanly separated from urbanisation-driven warming at the station scale, a limitation discussed in Chapter 5. What is established here is that both mean temperature and extreme heat frequency increased significantly over the study period, and that both series show a structurally distinct post-2010 trajectory.

4.2 Spatial Distribution of Extreme Heat: Four Temporal Snapshots

Inverse distance weighting interpolation was applied to the 26-station annual heat day totals for four representative years (2000, 2008, 2016, and 2024) to produce continuous spatial fields across the study area (Figure 4.2). The power parameter p = 2 was selected through leave-one-out cross-validation as the value minimising root mean squared error. The resulting surfaces are best interpreted at the scale of sub-regional gradients rather than local precision, particularly in the hilly terrain of southwestern Zhejiang and southern Anhui where IDW cannot account for elevation-driven temperature lapse rates.

In 2000, the spatial pattern was characterised by two contrasting zones. A broad inland arc of elevated heat burden, encompassing the western Zhejiang cities of Jinhua (37 days), the Anhui corridor cities of Ma'anshan (33 days), Wuhu (31 days), and Tongling (31 days), and extending southwest toward Anqing and Chizhou, recorded heat day counts consistently above 25 days. Concurrently, the northern coastal fringe of Jiangsu— Yancheng (11 days) and to a lesser extent Nantong and Zhenjiang— recorded substantially lower values. Shanghai (21 days) and most Jiangsu cities sat at intermediate levels. The regional mean in 2000 was 23.2 days.

By 2008, the regional mean had changed little (22.4 days), and the broad spatial structure visible in 2000 remained largely intact. The year 2008 was a relatively moderate heat season across the YRD: no city exceeded 31 days, the maximum recorded by Anqing. Jinhua, which had topped the 2000 distribution, fell to 20 days in 2008. This reversal illustrates the capacity of interannual WPSH

variability to override longer-term trends in single years, and underscores why trend detection requires multi-decadal series rather than pairwise year comparisons. The spatial field in 2008 therefore represents a year within the first-period baseline rather than a structurally different pattern.

The 2016 snapshot captures the post-mutation phase and shows a more widespread elevation of heat burden. The regional mean had risen to 26.7 days. Jinhua again led with 38 days, followed by Ma'anshan (37 days) and Yangzhou (35 days)— the latter a new entrant at the upper end of the distribution and indicative of expanding heat exposure along the Jiangsu corridor. Shanghai recorded 24 days in 2016, 3 days above its 2000 value but still well below the inland maximum. Yancheng remained an outlier at the low end (15 days), its coastal position continuing to suppress extreme maximum temperatures. The spatial contrast between the inland heat core and the northeastern coastal fringe persisted, but the gap between them had narrowed as Jiangsu corridor cities warmed more steeply.

In 2024, the regional mean reached 28.7 days, the second highest annual value in the record after 2022. Chuzhou emerged as the highest-heat city with 42 days, followed by Tongling and Ma'anshan (both 38 days). The Anhui cluster as a whole showed substantially elevated values relative to 2000. Shanghai recorded 22 days, modestly above its 2000 baseline. The northeastern coastal fringe continued to record the lowest values: Yancheng (20 days), Nantong and Taizhou-JS (both 19 days). Anqing recorded only 19 days, an anomalous low given its 2011–2024 period mean of 29.9 days and its significant upward trend ($\beta = 0.461$ days yr^{-1}). A single-year departure of this magnitude (approximately 11 days below the period mean) is consistent with year-specific synoptic suppression, such as an anomalous southward displacement of the WPSH axis or enhanced typhoon-related cloud cover during the peak heat season; the specific mechanism in 2024 would require synoptic analysis beyond the scope of this study. The 2024 spatial field does not show a simple expansion of a single heat core but rather a generalised intensification across the inland arc, with certain Jiangsu cities also approaching or exceeding 30 days for the first time.

Figure 4.2 Spatial distribution of annual high-temperature days (IDW, p = 2, 26 stations)

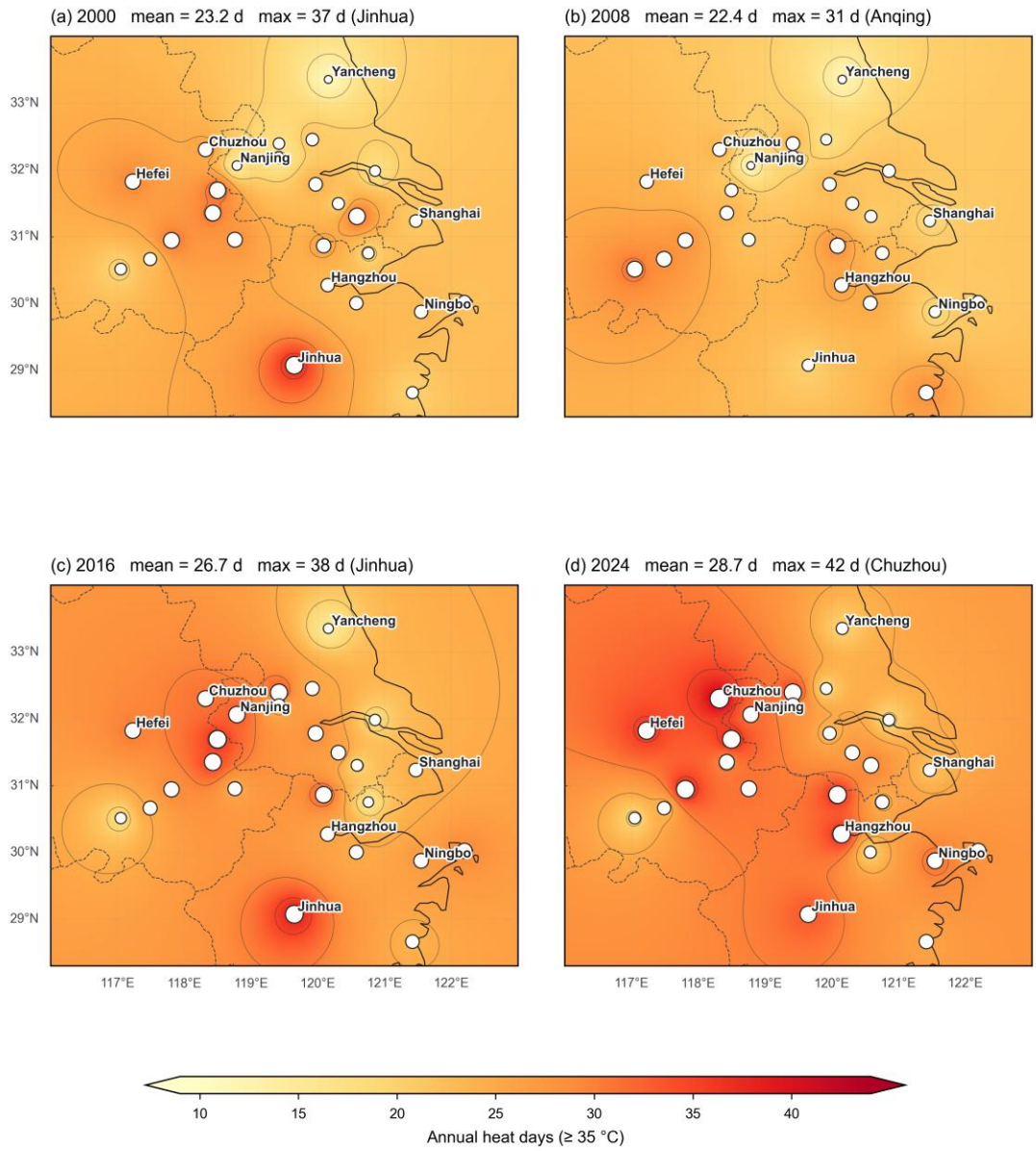

Figure 4.2. Spatial distribution of annual high-temperature days (≥35°C) across the Yangtze River Delta in 2000, 2008, 2016, and 2024, derived by inverse distance weighting (p = 2) from 26 meteorological stations. Station locations are shown as filled circles scaled to observed values. Colour scale is uniform across all panels (6–48 days). Dashed grey lines indicate approximate inter-provincial boundaries. Station abbreviations: SH = Shanghai; NJ = Nanjing; HF = Hefei; HZ = Hangzhou; JH = Jinhua; YC = Yancheng; CHU = Chuzhou; NB = Ningbo; AQ = Anqing; WX = Wuxi; SZ = Suzhou; WH = Wuhu; HU = Huzhou; JX = Jiaxing; SX = Shaoxing; CZ = Changzhou; YZ = Yangzhou; NT = Nantong; ZJ = Zhenjiang; TZ-JS = Taizhou (Jiangsu); TZ-ZJ = Taizhou (Zhejiang); ZS = Zhoushan; MAS = Ma'anshan; TL = Tongling; CHI = Chizhou; XC = Xuancheng.

4.3 City-Level Trend Analysis

4.3.1 Mann-Kendall Significance and Sen's Slope Estimates: Heat Days

Table 4.1 presents the Mann-Kendall Z statistic, p-value, Sen's slope, and inter-period mean comparison for each of the 26 cities. Of the 26 cities, 12 produced statistically significant upward trends in annual heat day frequency ($p < 0.05$), while 14 did not reach significance at that threshold. No city produced a statistically significant downward trend. The result for Tongling is the sole case with a negative Sen's slope ($\beta = -0.154$ days per year), though it is not significant ($Z = -0.632$, $p = 0.527$); Tongling's heat day count at the start of the record (28.7 days per year in 2000–2010) and negligible change across the two periods leave it as an outlier at the lower end of trend magnitudes.

Among the 12 significant cities, Sen's slope estimates range from 0.200 days per year (Taizhou-JS) to 0.588 days per year (Jinhua). The three steepest slopes belong to Jinhua (Zhejiang, 0.588), Nanjing (Jiangsu, 0.551, non-significant at p = 0.052), and Chuzhou (Anhui, 0.531). The two-period mean comparison shows that Jinhua experienced the largest absolute shift, with the inter-period mean rising from 26.1 days (2000–2010) to 36.1 days (2011–2024), a difference of 10.1 days. Changzhou recorded the next largest absolute shift (+7.9 days), followed by Shanghai, Zhoushan, and Chuzhou (all +7.4 days).

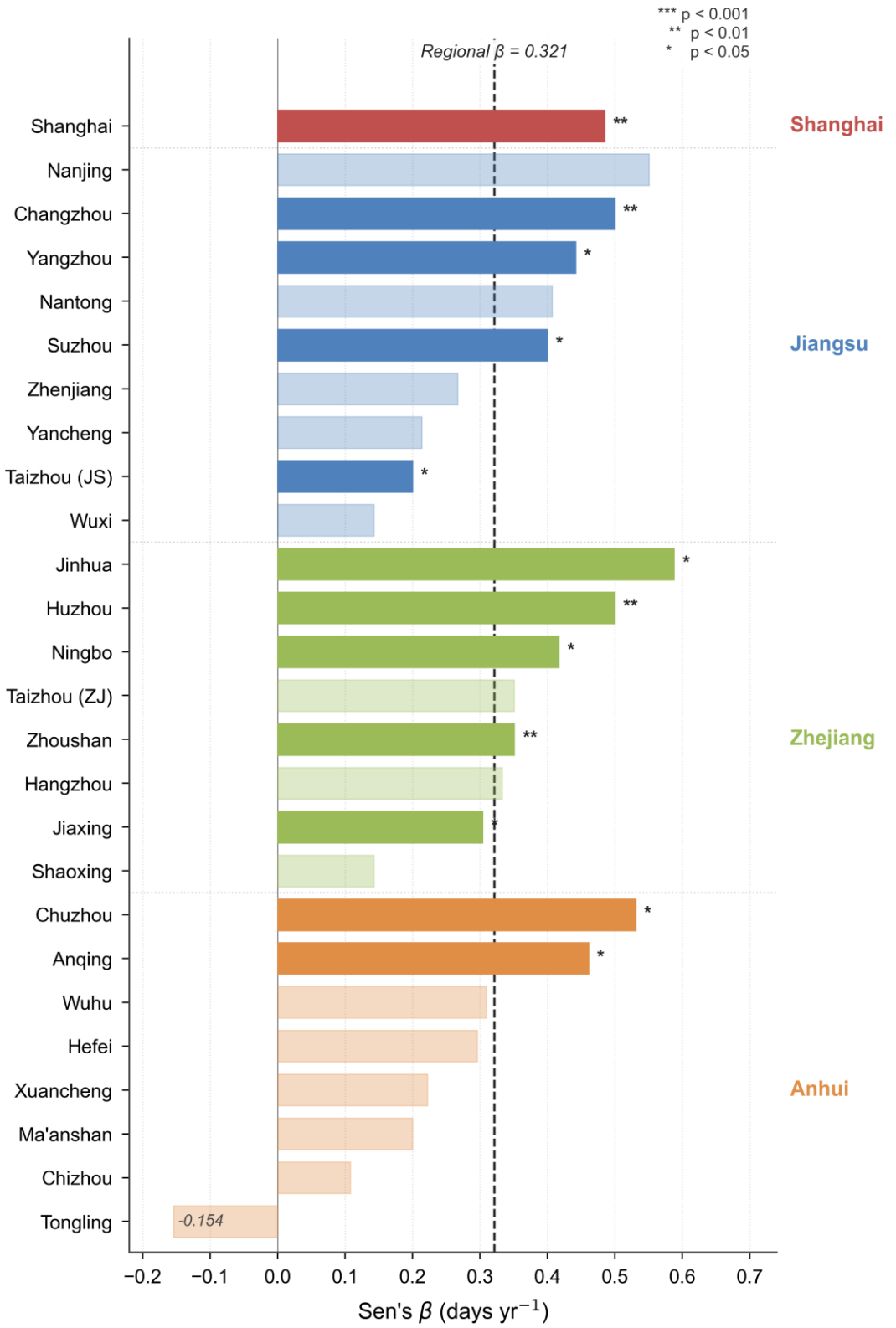

*Figure 4.3 visualises the full distribution of city-level Sen's slope estimates, grouped by province. The contrast between significant and non-significant cities within the same province is notable. Within Jiangsu, for example, Changzhou (0.500, *) and Yangzhou (0.442,) show steep slopes while Wuxi (0.143, ns) and Yancheng (0.214, ns) do not. Within Anhui, Chuzhou (0.531,) and Anqing (0.461,) are significant*

while Chizhou (0.108, ns), Xuancheng (0.222, ns), and Tongling (−0.154, ns) are not. This within-province heterogeneity indicates that provincial-level aggregation obscures substantial city-level variation in heat day accumulation rates.

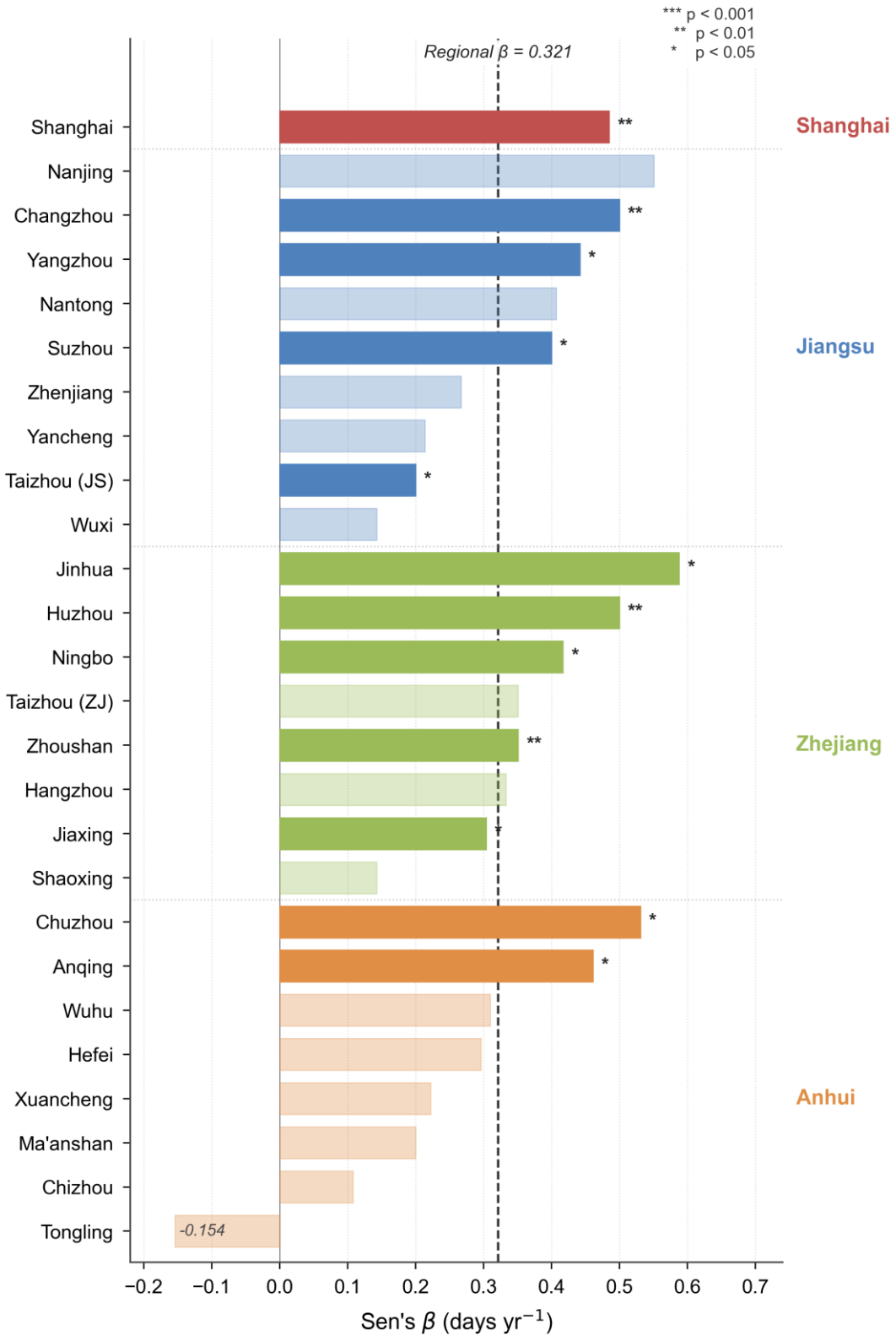

*Figure 4.3. Sen's slope estimates for annual high-temperature days by city, 2000–2024. Full-opacity bars indicate statistically significant trends ($p < 0.05$); faded bars indicate non-significant results. The vertical dashed line marks the 26-city regional mean slope (0.321 days yr−1). Cities are grouped by province. Sig. codes: * $p <$ 0.01, $p < 0.05$, ns = not significant.*

*Table 4.1. City-level Mann-Kendall test results and Sen's slope estimates for annual high-temperature days, 2000–2024. Period means calculated for 2000–2010 and 2011–2024. Significance codes: * $p < 0.01$, $p < 0.05$, ns = not significant.*

City	Province	Sen's β (days yr⁻¹)	p-value	Sig.	Δ (days)
Shanghai	Shanghai	0.485	0.002	**	+7.4
Nanjing	Jiangsu	0.551	0.052	ns	+6.8
Changzhou	Jiangsu	0.500	0.004	**	+7.9
Yangzhou	Jiangsu	0.442	0.028	*	+6.6
Nantong	Jiangsu	0.407	0.052	ns	+4.4
Suzhou	Jiangsu	0.400	0.029	*	+5.2
Zhenjiang	Jiangsu	0.267	0.240	ns	+3.4
Yancheng	Jiangsu	0.214	0.205	ns	+1.4
Taizhou (JS)	Jiangsu	0.200	0.028	*	+4.1
Wuxi	Jiangsu	0.143	0.237	ns	+2.8
Jinhua	Zhejiang	0.588	0.016	*	+10.1
Huzhou	Zhejiang	0.500	0.003	**	+6.7
Ningbo	Zhejiang	0.417	0.012	*	+6.9
Taizhou (ZJ)	Zhejiang	0.351	0.071	ns	+5.3
Zhoushan	Zhejiang	0.351	0.009	**	+7.4
Hangzhou	Zhejiang	0.333	0.054	ns	+2.6
Jiaxing	Zhejiang	0.304	0.046	*	+3.2
Shaoxing	Zhejiang	0.143	0.360	ns	+0.9
Chuzhou	Anhui	0.531	0.011	*	+7.4
Anqing	Anhui	0.461	0.024	*	+3.8
Wuhu	Anhui	0.310	0.086	ns	+6.5
Hefei	Anhui	0.296	0.060	ns	+5.2
Xuancheng	Anhui	0.222	0.087	ns	+1.8
Ma'anshan	Anhui	0.200	0.241	ns	+4.9
Chizhou	Anhui	0.108	0.622	ns	+1.5
Tongling	Anhui	-0.154	0.527	ns	-0.5

4.3.2 Provincial Patterns and Intra-Provincial Heterogeneity

When city-level Sen's slopes are aggregated to the provincial level, Jiangsu cities average 0.347 days per year (range: 0.143 to 0.551), Zhejiang cities average 0.373 days per year (range: 0.143 to 0.588), and Anhui cities average 0.247 days per year (range: −0.154 to 0.531). Shanghai, as a single-city province, records 0.485 days per year. The Zhejiang mean slope is marginally steeper than Jiangsu's, driven by

Jinhua and Huzhou. Anhui's lower mean reflects the high inter-period baseline values of its southern cities (Tongling, Chizhou, Xuancheng) in 2000–2010, leaving less room for statistically detectable upward drift, rather than a slower underlying warming rate.

The inter-period comparison is informative in this regard. All Anhui cities except Tongling show positive differences between the two-period means, but the magnitudes in the southernmost Anhui cities (Chizhou +1.5 days, Xuancheng +1.8 days) are small relative to those of Chuzhou (+7.4 days) or Ma'anshan (+4.9 days). The implication is that cities which were already at high absolute heat levels in 2000–2010 have shown smaller incremental shifts, while cities that began the period at intermediate levels have accumulated heat days more rapidly. This pattern is consistent with the non-linear saturation argument advanced by Zhai et al. (2020) in the context of built-up area and heat island intensity.

4.3.3 Annual Mean Temperature Trends by City

Annual mean temperature trends (Table 4.2) show a higher rate of statistical significance than heat day trends: 23 of 26 cities record significant positive warming ($p < 0.05$), and 7 reach $p < 0.001$. Sen's slope estimates for temperature range from 0.013°C per year (Chuzhou, non-significant) to 0.063°C per year (Ningbo). The highest slopes are found in coastal and estuarine cities: Ningbo (0.063°C yr−1), Nanjing (0.061°C yr−1), and Nantong (0.055°C yr−1). In contrast, several inland Anhui cities record the lowest temperature Sen's slopes (Chuzhou 0.013, Yancheng 0.015), cities that also tended to record the lowest significance levels in the heat day analysis.

The divergence between temperature trend significance (23/26 cities) and heat day trend significance (12/26 cities) is expected given the measurement properties of each variable. Annual mean temperature is derived from 365 daily means and is thus a relatively stable statistic with low year-to-year variance, making monotonic trends easier to detect. Annual heat day counts are bounded below by zero, exhibit high right skew in years with active WPSH, and can shift dramatically between years for reasons unrelated to long-term forcing. The Mann-Kendall test is therefore more likely to achieve significance for the temperature variable given the same underlying forcing signal.

Two city-level cases illustrate this divergence in instructive ways. Chuzhou recorded one of the steepest heat day Sen's slopes in the dataset (0.531 days yr^{-1}, p = 0.011) but the weakest annual mean temperature trend (0.013°C yr^{-1}, p = 0.129). This combination is physically plausible if warming at Chuzhou has been concentrated in the upper tail of the summer temperature distribution rather than distributed evenly across the annual cycle. A small shift in the daily maximum temperature distribution near the 35°C threshold can produce a large change in the number of days exceeding that threshold without substantially altering the annual mean. Chizhou presents the inverse pattern: a highly significant temperature trend (0.050°C yr^{-1}, p < 0.001) but negligible heat day trend (0.108 days yr^{-1}, p = 0.622). Here the warming appears to have been distributed broadly across the temperature distribution, raising the mean without pushing enough additional days past the 35°C threshold to register as a trend in heat day counts. These contrasting cases reinforce the point that annual mean temperature and extreme heat day frequency are related but distinct indicators, and that trends in one should not be assumed to imply equivalent trends in the other.

Table 4.2. City-level Mann-Kendall test results and Sen's slope estimates for annual mean temperature, 2000–2024. Significance codes: ***p < 0.001,** *p < 0.01, * p < 0.05, ns = not significant.*

City	Province	Sen's β (°C yr^{-1})	p-value	Sig.
Nanjing	Jiangsu	0.0610	<0.001	***
Nantong	Jiangsu	0.0553	<0.001	***
Jinhua	Zhejiang	0.0487	<0.001	***
Ningbo	Zhejiang	0.0629	<0.001	***
Jiaxing	Zhejiang	0.0541	<0.001	***
Chizhou	Anhui	0.0497	<0.001	***
Shanghai	Shanghai	0.0318	0.003	**
Wuxi	Jiangsu	0.0152	0.059	ns
Yancheng	Jiangsu	0.0145	0.118	ns
Chuzhou	Anhui	0.0134	0.129	ns

4.4 Socioeconomic Correlations with Extreme Heat Frequency

4.4.1 Cross-Sectional Spearman Correlations

Spearman rank correlations were computed between city-mean annual heat day frequency and each of the three socioeconomic indicators— built-up area, permanent resident population, and per capita GDP across 26 cities using mean

values for the 2000–2023 overlap period (Table 4.3, Figure 4.4). All three correlations are statistically significant at $p < 0.01$ but in the negative direction, contrary to the positive associations anticipated from the literature. Heat days correlate negatively with built-up area ($\rho = -0.572$, $p = 0.002$), negatively with population ($\rho = -0.520$, $p = 0.006$), and negatively with per capita GDP ($\rho = -0.585$, $p = 0.002$).

The direction of these correlations is driven by a geographic confound inherent to the spatial structure of the YRD dataset. The cities with the highest heat day means are predominantly inland: Jinhua (31.7 days, mean per capita GDP 47,916 yuan), Chuzhou (29.6 days, 32,047 yuan), Xuancheng (28.7 days, 32,069 yuan), and Anqing (28.6 days, 27,010 yuan). These inland cities have below-average per capita GDP, relatively small built-up areas, and lower populations. Conversely, the cities with the highest per capita GDP and built-up area are predominantly coastal or near-coastal: Shanghai (96,347 yuan, 985 km² built-up, 20.3 heat days), Suzhou (113,543 yuan, 360 km², 23.7 heat days), and Wuxi (113,388 yuan, 274 km², 22.1 heat days). The coastal maritime influence that moderates summer maximum temperatures in these cities is also the primary reason they record fewer heat days than inland counterparts at equivalent or higher latitudes.

The negative cross-sectional correlation is therefore a consequence of the co-linearity between coastal location, economic development level, and maritime climate moderation, rather than a causal relationship between urbanisation and heat. This is precisely the geographic confound that station-based cross-sectional correlation analysis cannot resolve without controlling for baseline climatic exposure. Panel analyses on first-differenced variables examining whether year-on-year increases in built-up area or GDP within each city were associated with year-on-year increases in heat days produced Spearman coefficients near zero and far from significance ($\rho = 0.028$ for built-up area, $\rho = 0.007$ for GDP, $\rho = 0.044$ for population; all $p > 0.28$). Similarly, city-level Sen's slope estimates for heat days did not correlate significantly with mean socioeconomic levels across the 26 cities ($\rho = 0.245$ for built-up area, $p = 0.227$). These additional analyses collectively indicate that the cross-sectional negative correlation is a spatial confound rather than a stable empirical relationship.

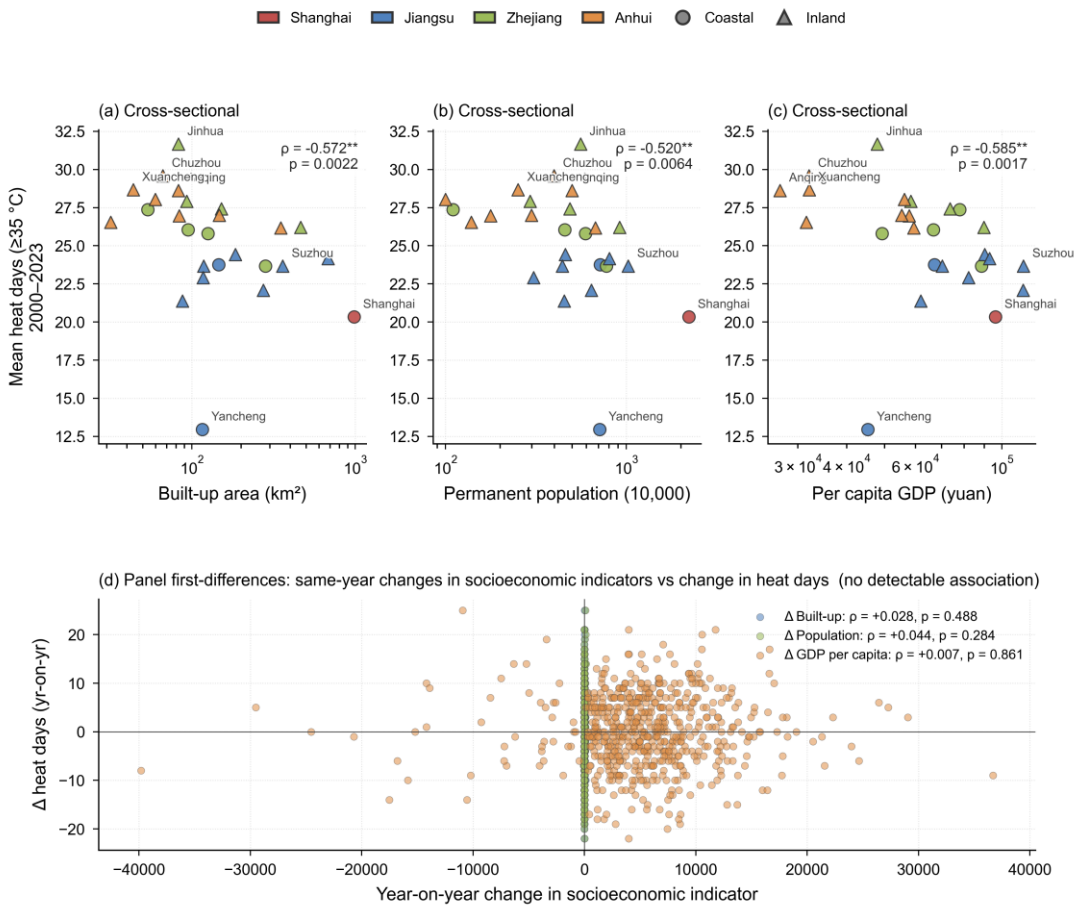

*Figure 4.4. Spearman rank correlations between city-mean annual high-temperature days (2000–2023) and three socioeconomic indicators across 26 YRD cities. (a–c) Cross-sectional view: each point is one city, coloured by province (red, Shanghai; blue, Jiangsu; green, Zhejiang; orange, Anhui); circles denote coastal cities (within roughly 50 km of the coast or estuary) and triangles denote inland cities. Built-up area and per capita GDP are plotted on logarithmic axes to accommodate right-skewed distributions. Inset boxes report Spearman ρ and two-tailed p-values. (d) Panel first-difference view: same-year changes in each socioeconomic indicator versus same-year change in annual heat days, pooled across all city–year transitions; near-zero coefficients show that the cross-sectional negative associations in (a–c) do not survive within-city differencing. ** $p < 0.01$.*

*Table 4.3. Spearman rank correlations between city-mean annual heat days and socioeconomic indicators, 2000–2023 (n = 26 cities). ** $p < 0.01$.*

Variable pair	Spearman ρ	p-value	Significance	Interpretation
Heat days × Built-up area	-0.572	0.002	**	Negative; coastal–inland confound
Heat days × Population	-0.520	0.006	**	Negative; coastal–inland confound
Heat days × Per	-0.585	0.002	**	Negative;

capita GDP				coastal–inland confound

4.4.2 Implications of the Correlation Structure for Interpretation

The result returned by this analysis— statistically significant negative correlations between all three socioeconomic variables and heat day frequency— is internally consistent and reproducible from the data as structured. What it does not do is resolve the theoretical question that motivated the analysis: whether economic output, population scale, or built-up land area most strongly amplifies extreme heat at the city level in the YRD. The cross-sectional design conflates baseline climatic exposure with socioeconomic development, and the two cannot be separated without either controlling for geographic position (e.g., through distance from coast or elevation) or using a research design that holds climate constant while varying the socioeconomic predictor. Neither is feasible at the scale and data resolution of this study. I argue this confound is precisely the caveat I flagged in §3.6.2.

The hypothesised positive association between urbanisation indicators and heat frequency, which the literature predicts at the intra-city scale (Oke, 1982; Hao et al., 2018; Li et al., 2024), does not manifest as a detectable cross-sectional signal at the inter-city scale in the YRD when the coastal–inland climatic gradient runs systematically counter to the urbanisation gradient. The negative correlation is an artefact of that spatial structure. Its direction is predictable given the data configuration, which is itself the justification for reporting the panel first-difference analysis alongside the cross-sectional results. The absence of significant panel correlations suggests that short-run year-to-year changes in socioeconomic variables do not produce detectable same-year changes in heat day frequency, consistent with the expectation that urban surface modification effects on climate operate over decadal rather than annual timescales (Zhou and Qian, 2021).

4.5 Summary

Four findings emerge from the analysis and are carried into the Discussion. First, the YRD experienced a statistically significant increase in regional mean annual high-temperature days over 2000–2024 ($Z = 4.906$, $p < 0.001$), with a Sen's slope of 0.321 days per year and a structural break near 2010–2011 after which the

trend intensified. Second, the spatial distribution of heat burden is not geographically uniform: an inland arc spanning western Zhejiang and northern Anhui consistently recorded the highest heat day totals, while the northeastern coastal fringe of Jiangsu recorded the lowest, and this spatial structure persisted across all four snapshot years. Third, city-level trend magnitudes vary substantially: 12 of 26 cities show significant positive trends in heat day frequency, the steepest being Jinhua (0.588 days yr−1) and Chuzhou (0.531 days yr−1), while 14 cities, including several in southern Anhui, do not reach significance despite high absolute heat levels. Fourth, cross-sectional Spearman correlations between heat day frequency and socioeconomic indicators are all negative and statistically significant, an outcome driven by the geographic confound between coastal location, economic development, and maritime climate moderation; panel first-difference correlations are uniformly near zero, indicating no detectable short-run within-city association between annual changes in socioeconomic variables and annual changes in heat day frequency. I interpret the implications of these four findings for heat-adaptation planning in Chapter 5.

Appendix A — Full city-level statistical tables

The two tables below report the complete Mann-Kendall and Sen's slope statistics for all 26 cities. Compressed forms of these tables appear in the main text as Table 4.1 and Table 4.2; the main-text versions retain the columns most directly used in the analytical narrative, while the present appendix provides the full set of statistics for reference.

Table A1. Full city-level Mann-Kendall and Sen's slope statistics for annual high-temperature days, 2000–2024. Period means calculated for 2000–2010 and 2011–2024. Significance codes: * $p < 0.01$, $p < 0.05$, ns = not significant.

City	Province	MK Z	p-value	Sen's β (days yr⁻¹)	Sig.	Mean 2000–10	Mean 2011–24	Δ (days)
Shanghai	Shanghai	+3.173	0.002	0.485	**	16.3	23.6	+7.4
Nanjing	Jiangsu	+1.946	0.052	0.551	ns	20.6	27.4	+6.8
Changzhou	Jiangsu	+2.857	0.004	0.500	**	19.9	27.9	+7.9
Yangzhou	Jiangsu	+2.202	0.028	0.442	*	20.5	27.1	+6.6
Nantong	Jiangsu	+1.942	0.052	0.407	ns	21.1	25.5	+4.4
Suzhou	Jiangsu	+2.185	0.029	0.400	*	21.0	26.2	+5.2
Zhenjiang	Jiangsu	+1.174	0.240	0.267	ns	21.2	24.6	+3.4
Yancheng	Jiangsu	+1.269	0.205	0.214	ns	12.5	13.9	+1.4
Taizhou	Jiangsu	+2.197	0.028	0.200	*	19.0	23.1	+4.1

(JS)								
Wuxi	Jiangsu	+1.181	0.237	0.143	ns	20.7	23.5	+2.8
Jinhua	Zhejiang	+2.411	0.016	0.588	*	26.1	36.1	+10.1
Huzhou	Zhejiang	+3.004	0.003	0.500	**	24.5	31.2	+6.7
Ningbo	Zhejiang	+2.511	0.012	0.417	*	20.1	27.0	+6.9
Taizhou (ZJ)	Zhejiang	+1.805	0.071	0.351	ns	22.8	28.1	+5.3
Zhoushan	Zhejiang	+2.627	0.009	0.351	**	23.3	30.6	+7.4
Hangzhou	Zhejiang	+1.925	0.054	0.333	ns	25.2	27.8	+2.6
Jiaxing	Zhejiang	+1.991	0.046	0.304	*	24.2	27.4	+3.2
Shaoxing	Zhejiang	+0.916	0.360	0.143	ns	26.6	27.5	+0.9
Chuzhou	Anhui	+2.555	0.011	0.531	*	25.9	33.4	+7.4
Anqing	Anhui	+2.256	0.024	0.461	*	26.1	29.9	+3.8
Wuhu	Anhui	+1.715	0.086	0.310	ns	23.5	29.9	+6.5
Hefei	Anhui	+1.883	0.060	0.296	ns	23.6	28.9	+5.2
Xuancheng	Anhui	+1.714	0.087	0.222	ns	27.7	29.6	+1.8
Ma'anshan	Anhui	+1.172	0.241	0.200	ns	24.6	29.6	+4.9
Chizhou	Anhui	+0.493	0.622	0.108	ns	25.5	27.1	+1.5
Tongling	Anhui	-0.632	0.527	-0.154	ns	28.7	28.2	-0.5

Table A2. Full city-level Mann-Kendall and Sen's slope statistics for annual mean temperature, 2000–2024. Significance codes: * **p < 0.001,** p < 0.01, * p < 0.05, ns = not significant.

City	Province	MK Z	p-value	Sen's β (°C yr^{-1})	Sig.
Shanghai	Shanghai	+2.966	0.003	0.0318	**
Nanjing	Jiangsu	+3.994	<0.001	0.0610	***
Nantong	Jiangsu	+4.227	<0.001	0.0553	***
Taizhou (JS)	Jiangsu	+3.246	0.001	0.0335	**
Suzhou	Jiangsu	+2.546	0.011	0.0319	*
Changzhou	Jiangsu	+2.265	0.024	0.0318	*
Zhenjiang	Jiangsu	+2.312	0.021	0.0228	*
Wuxi	Jiangsu	+1.892	0.059	0.0152	ns
Yangzhou	Jiangsu	+1.705	0.088	0.0161	ns
Yancheng	Jiangsu	+1.565	0.118	0.0145	ns
Jinhua	Zhejiang	+3.713	<0.001	0.0487	***
Ningbo	Zhejiang	+4.181	<0.001	0.0629	***
Jiaxing	Zhejiang	+4.112	<0.001	0.0541	***
Shaoxing	Zhejiang	+3.153	0.002	0.0457	**
Hangzhou	Zhejiang	+2.546	0.011	0.0343	*
Huzhou	Zhejiang	+2.873	0.004	0.0406	**
Taizhou (ZJ)	Zhejiang	+2.452	0.014	0.0285	*
Zhoushan	Zhejiang	+1.869	0.062	0.0281	ns
Hefei	Anhui	+2.243	0.025	0.0250	*
Anqing	Anhui	+3.153	0.002	0.0408	**
Wuhu	Anhui	+2.639	0.008	0.0293	**

Ma'anshan	Anhui	+2.359	0.018	0.0401	*
Xuancheng	Anhui	+2.265	0.024	0.0292	*
Tongling	Anhui	+2.032	0.042	0.0254	*
Chizhou	Anhui	+3.527	<0.001	0.0497	***
Chuzhou	Anhui	+1.518	0.129	0.0134	ns

Chapter 5: Discussion

The four findings reported in Chapter 4 establish that extreme heat in the Yangtze River Delta has intensified across the period 2000–2024, that the intensification is spatially uneven and follows the region's coastal–inland geography, and that the cross-sectional association between socioeconomic indicators and heat day frequency is dominated by a geographic confound rather than by a causal mechanism. This chapter interprets these findings in the context of the literature reviewed in Chapter 2, identifies the mechanisms that most plausibly explain them, and engages directly with the limits of what station-based observational analysis can establish. Section 5.1 places the regional warming signal in its broader Chinese and global context. Section 5.2 considers candidate mechanisms for the 2010–2011 structural break. Section 5.3 develops what I term the spatial paradox of YRD heat: the inversion of expected heat geography relative to economic geography. Section 5.4 develops the methodological implications of the socioeconomic confound, which I argue is the most generalisable contribution of this study. Section 5.5 outlines adaptation-planning implications. Sections 5.6 and 5.7 acknowledge limitations and identify future research directions.

5.1 Regional Warming in Context

In §4.1 I reported a regional Sen's slope of 0.321 days per year for annual heat day frequency (MK $Z = 4.906$, $p < 0.001$) and 0.036 °C per year for annual mean temperature ($Z = 5.862$, $p < 0.001$), giving cumulative trends across the 25-year window of approximately 7.7 additional heat days and 0.85 °C of warming. These figures sit at the upper end of what the recent literature reports for the broader Chinese subtropical zone.

Zheng et al. (2021), in their analysis of extreme temperature indices across China's six climate zones for 1961–2020, identified the northern subtropical zone (the band encompassing the YRD) as exhibiting the steepest acceleration in warm extreme indices over the most recent two decades. Their reported rates for hot day frequency in the northern subtropical zone of roughly 0.27 to 0.31 days per year for the post-2000 sub-period are broadly consistent with the 0.321 days per year I obtain for the YRD-26 aggregate. The convergence is reassuring: my dataset, restricted to

the State Council 2016 boundary and drawing on 26 specific municipal stations, recovers a regional signal consistent with the much larger station network used in the national synthesis.

A useful comparator is Huang and Lu (2015), who reported a UHI-attributable warming rate of approximately 0.483 °C per decade for large YRD cities (≈ 0.048 °C per year) and 0.179 °C per decade (≈ 0.018 °C per year) for smaller peripheral cities. My 0.036 °C per year for the 26-city aggregate sits squarely between these two estimates, which is what one would expect if the aggregate is a weighted average of large coastal cities and smaller inland ones. The agreement at this coarse level lends credibility to the dataset; it does not, however, allow me to attribute any specific fraction of the warming to urbanisation versus background forcing, a point I return to in §5.6.

The cumulative figure of 7.7 additional heat days over 25 years is worth restating in terms an adaptation planner can use. If the regional Phase I mean was 22.7 heat days per year and the Phase II mean is 27.5, the effective heat season has lengthened by roughly five days, equivalent in some years to extending a typical July heatwave by an additional week. This is not a marginal climate signal. Cities such as Jinhua, where the inter-period shift was 10.1 days, have effectively gained more than a fortnight of new heat exposure within a single generation.

I argue, therefore, that the regional warming signal recovered here is not an artefact of station choice or analytical decisions: it is consistent with national-scale literature, internally coherent across the two related variables (heat day frequency and mean temperature), and large enough to register as policy-relevant rather than statistically academic.

5.2 The 2010–2011 Structural Break: Candidate Mechanisms

The sequential Mann-Kendall analysis in §4.1.1 located a probable mutation point near 2010–2011, with the forward statistic UF crossing the 1.96 confidence boundary in 2011 and reaching 5.80 by 2024. The two-period mean comparison gave 22.7 heat days for 2000–2010 and 27.5 heat days for 2011–2024, a 21 per cent increase. Identifying the mechanism behind this break is more difficult than identifying the break itself, and three candidate mechanisms warrant consideration.

The first candidate is a shift in the behaviour of the Western Pacific Subtropical High (WPSH). Ding et al. (2010) established that WPSH variability is the dominant interannual control on high-temperature day frequency across the Yangtze basin, and Wang et al. (2024), examining near-surface and surface urban heat island contrasts in the YRD, reported that the post-2010 period coincided with more frequent westward extensions of the WPSH over eastern China. If the WPSH entered a new regime around 2010–2011, with more frequent or persistent westward intrusions during the boreal summer, this alone could explain a step change in heat day frequency. The 2013 anomaly, widely documented as one of the most extreme heat summers on record for the YRD, would on this account be a particularly forceful manifestation of the new regime rather than an isolated event. The difficulty with this attribution is that station data cannot directly diagnose WPSH variability; reanalysis-based studies (Xie et al., 2017) suggest the WPSH change is real but do not isolate it from the second candidate mechanism.

The second candidate is an urbanisation-driven local amplification. Several lines of evidence in the literature point to a nonlinear relationship between built-up area expansion and surface energy modification: Zhai et al. (2020) showed that heat intensification per unit of built-up expansion is steeper during early phases of urbanisation and moderates during later infill, and Li et al. (2024), using XGBoost-SHAP attribution, identified built-up area as the dominant structural predictor of land surface temperature in the YRD. Between 2000 and 2010 the YRD's built-up area roughly doubled across most of the 26 cities. It is plausible that the cumulative effect of this expansion crossed a threshold around 2010, after which urban surface modification began to amplify the WPSH-driven signal rather than merely accompanying it.

The third candidate is the broader global warming acceleration identified in the IPCC AR6 (Zhou & Qian, 2021). The decade 2011–2020 was the warmest on the global instrumental record, and most of that warming was concentrated in the Northern Hemisphere mid-latitudes. The structural break in the YRD record may therefore reflect a regional manifestation of a global forcing change rather than anything intrinsic to the YRD.

I cannot adjudicate among these three mechanisms with the data available to this study. The honest position is that all three predict a discontinuity of

approximately the magnitude observed, that all three are individually well-supported in the literature, and that disentangling them requires a research design beyond the scope of what station observations alone can support. A definitive attribution would need, at minimum, coupled ERA5-based WPSH diagnostics, satellite-based built-up area tracking, and a forcing decomposition of the type IPCC AR6 attribution studies undertake. What I do establish here is that the break is real, that it occurred close to 2010–2011, and that the post-break regime has shown no sign of relaxation across the eight years of the post-2017 record.

5.3 Spatial Paradox: Inland Heat Core vs Coastal Moderation

The spatial findings in §4.2 and §4.3 yielded what at first inspection appears to be a paradox. The YRD's most economically developed cities (Shanghai, Suzhou, Wuxi, Ningbo) do not record the region's highest heat day counts. The highest counts are recorded in inland Zhejiang (Jinhua, repeatedly above 35 days) and the Anhui corridor (Chuzhou peaking at 42 days in 2024). The northeastern coastal fringe of Jiangsu (Yancheng, Nantong) records the lowest counts. This pattern persists across all four snapshot years and is consistent with the city-level Sen's slope distribution: the steepest accumulation rates also lie in Jinhua, Chuzhou, and Anqing, not in the coastal economic core.

This pattern runs counter to the intuition the UHI literature builds. Peng et al. (2012), in their global synthesis of 419 cities, found that surface UHI intensity scales with city size; Huang and Lu (2015) reported that large YRD cities warmed faster than peripheral cities in mean temperature terms. If both of these findings were directly applicable to heat day frequency, one would expect Shanghai to top the YRD distribution. It does not.

The resolution lies in distinguishing the variable being measured. Heat day frequency is a tail statistic of the daily maximum temperature distribution, sensitive to whether the daily Tmax exceeds 35 °C. Mean temperature, by contrast, integrates conditions across the entire 24-hour cycle and across all seasons. The mechanisms that drive these two variables are not identical. UHI effects are most prominent in nocturnal minimum temperatures and in surface (rather than near-surface) measurements; Wang et al. (2024) documented this distinction explicitly for the YRD. Daily maximum temperatures during summer afternoon hours, when air

mixing is at its diurnal maximum, are far more strongly influenced by synoptic forcing and by mesoscale atmospheric moisture distributions than by canopy-layer heat storage.

In the YRD specifically, two additional mechanisms compound the coastal–inland contrast. First, maritime advection from the East China Sea moderates afternoon temperatures along the coast. Sea surface temperatures in the western East China Sea peak at approximately 26 °C in late summer, well below the 35 °C heat day threshold, and onshore sea breezes act as a natural air conditioner during the hours when continental cities would otherwise approach or cross that threshold. The Hangzhou Bay cities (Ningbo, Zhoushan, Jiaxing) and the Yangtze estuary cities (Shanghai, Nantong) benefit from this advection most directly. Second, the urban dry island effect documented by Hao et al. (2018) operates with different intensity across the gradient. Inland cities with continuous impervious surfaces and low surrounding water area have suppressed latent heat fluxes and therefore higher Tmax for a given level of incoming radiation. Coastal cities, while also impervious, are surrounded by water bodies that buffer Tmax through evaporative cooling of the boundary layer.

The combination of these two mechanisms, maritime advection and a coastal break in the urban dry island, produces a geography in which extreme heat exposure runs counter to economic development. I argue that this inversion is not a curiosity but a stable feature of YRD climate that any future heat-exposure assessment must take into account. Crucially, this finding does not contradict the UHI literature: within Shanghai or within Suzhou, urban cores almost certainly experience more heat exposure than the surrounding rural land (Peng et al., 2012; Oke, 1982). What the data establish is that the gradient between coastal Shanghai and inland Jinhua is not a UHI gradient; it is a maritime gradient, and the UHI effect, where it operates, is operating on top of a larger climatic differential running in the opposite direction.

This is the resolution of the apparent paradox. The spatial heat field in the YRD is not telling us that economic development reduces heat. It is telling us that proximity to the East China Sea moderates extreme heat, and that the cities with the strongest economies happen, for historical and geographical reasons, to be on the coast.

5.4 The Socioeconomic Confound: What Cross-Sectional Correlation Cannot Tell Us

The most cited and possibly the most misleading finding of this study, taken at face value, is the set of cross-sectional Spearman correlations reported in §4.4: heat day frequency correlates negatively and significantly with built-up area ($\rho = -0.572$, $p = 0.002$), with permanent resident population ($\rho = -0.520$, $p = 0.006$), and with per capita regional GDP ($\rho = -0.585$, $p = 0.002$). A reader confronting these numbers without further context would conclude that economic development, urbanisation, and population concentration in the YRD reduce extreme heat exposure. This conclusion would be incorrect. It would also be in direct contradiction with a substantial international literature (Oke, 1982; Peng et al., 2012; Hao et al., 2018; Klein & Anderegg, 2021) that documents urban heat island effects at the intra-city scale. Reconciling the apparent contradiction is the methodological centrepiece of this thesis, and I argue here that the reconciliation has implications well beyond the YRD.

The first step is to distinguish the spatial scale at which a heat–urbanisation correlation is computed. The intra-city UHI claim, formalised by Oke (1982) and validated across hundreds of global cities by Peng et al. (2012), compares urban land cover to surrounding non-urban land cover within the same metropolitan footprint. At this scale, the maritime moderation effect described in §5.3 acts on both urban and non-urban land equivalently and therefore cancels out of the comparison. What remains is the energy balance modification produced by impervious surfaces, anthropogenic heat release, and reduced evapotranspiration, all of which operate to raise urban temperatures above rural baselines. This intra-city UHI relationship is real, well-established, and not contradicted by any finding in this thesis. I make no claim here that the UHI does not exist.

The inter-city comparison undertaken in §4.4 is structurally different. It compares 26 separate cities to one another across a coastal–inland gradient. As §5.3 established, this gradient is dominated by maritime advection, not by urbanisation. The cross-sectional correlation between, say, Shanghai's GDP and Shanghai's heat day count is being computed against Jinhua's GDP and Jinhua's heat day count, and the dominant differentiator between these two cities is not their socioeconomic status but their distance from the coast and their elevation. Per capita GDP and distance

from the coast are themselves strongly correlated in the YRD because the historical geography of Chinese coastal trade concentrated economic activity in port cities. The cross-sectional Spearman coefficient is therefore not isolating the relationship between urbanisation and heat; it is measuring a composite signal in which the geographic confound dominates.

This is a textbook instance of what the spatial epidemiology literature calls confounding by spatial gradient, and what the ecological inference literature would call an ecological fallacy if the inferred causal direction were reversed. The cross-sectional design simply cannot answer the underlying causal question. The two interpretively viable conclusions I can draw from the cross-sectional correlations are: first, that across the 26 YRD cities, more economically developed cities happen to have fewer heat days; and second, that this descriptive co-occurrence offers no information about the causal effect of economic development on heat. Strong claims about the direction or magnitude of any causal effect require a different analytical design.

The panel first-difference analysis I report in §4.4.1 is one such design. By computing year-on-year changes in heat days within each city and correlating these against year-on-year changes in socioeconomic indicators within the same city, the geographic position of each city is held constant. Whatever maritime moderation effect operates on Shanghai's annual heat days does so equally on Shanghai's 2008 and 2009 values, and therefore disappears from the differenced comparison. The panel coefficients I obtained were $\rho = 0.028$ for built-up area, $\rho = 0.044$ for population, and $\rho = 0.007$ for per capita GDP, all far from statistical significance. These near-zero panel coefficients are not direct evidence that urbanisation fails to amplify heat days. The relevant timescale of urban surface energy balance modification is likely longer than one year (Zhou & Qian, 2021). What they do establish is that within-city year-on-year fluctuation in socioeconomic indicators does not produce detectable contemporaneous change in heat day frequency at the YRD scale.

The methodological implication is broader than the YRD. Any regional comparative study that draws cross-sectional inferences about urbanisation–heat relationships across a spatial gradient that also varies in baseline climate exposure is vulnerable to the same confound. Coastal megaregions in southern China (Pearl

River Delta, with Hong Kong–Shenzhen–Guangzhou), in Japan (Tokyo–Yokohama–Osaka), and in the United States (Boston–New York–Washington corridor) all share the structural property that their most economically developed cities are also their most climatically moderated cities. A naive cross-sectional Spearman or Pearson correlation in any of these settings will tend to recover negative coefficients between socioeconomic indicators and heat exposure, and a naive reading of those coefficients will tend to mislead.

The corrective is structural. Cross-sectional analyses in such regions should either explicitly control for geographic position (through covariates such as distance to coast, elevation, or latitude), or should be supplemented by within-city panel designs that hold geography constant. I argue that the present study's most generalisable contribution is the demonstration that these two designs, applied to the same dataset, yield qualitatively opposite-looking results, and that the cross-sectional design is the one to discount.

This argument also clarifies what this thesis does not establish. I have not shown that urbanisation in the YRD has no effect on heat day frequency. The panel coefficients near zero are informative about short-run within-city associations only. Multi-decadal urban surface modification may well amplify heat day frequency at timescales of 10 to 30 years through cumulative mechanisms that no annual panel can detect. Studies designed to detect such effects, such as longitudinal comparisons of paired cities at matched climatic baseline, or quasi-experimental analyses of cities whose urbanisation trajectories diverged for exogenous reasons, remain the appropriate vehicle for that question. The contribution of this thesis is to specify what cross-sectional Spearman cannot tell us about that question, and to provide a worked example of how the geographic confound operates in a real dataset.

5.5 Implications for Heat-Adaptation Planning

Three implications follow from the findings of this thesis for heat-adaptation planning in the YRD.

First, spatial targeting of adaptation resources should follow the heat day distribution, not the population or economic development distribution. The cities with the highest absolute heat exposure (Jinhua, Chuzhou, Anqing, and the broader

inland Anhui corridor) are not the cities with the largest adaptation budgets, the most developed health infrastructure, or the most active adaptation planning communities. Shanghai, Suzhou, and Hangzhou dominate adaptation discourse and funding flows within the YRD, but the data establish that their heat exposure is lower than that of several inland secondary cities. I argue that adaptation policy in the YRD has wrongly inherited the megacity-centric intuition from the international UHI literature, and that a reallocation of attention toward inland secondary cities is overdue.

Second, the inland Anhui cities are the most vulnerable to future trajectories. These cities combine high absolute heat exposure with rapid ongoing built-up area expansion: the period 2000–2023 saw the most aggressive proportional urban growth across the YRD concentrated precisely in cities like Chuzhou, Anqing, and Xuancheng. While the panel first-difference results in §4.4 found no detectable short-run within-city association between socioeconomic change and heat days, the multi-decadal urban surface modification literature (Hao et al., 2018; Zhai et al., 2020) suggests that cumulative effects do operate at longer timescales. Continued built-up expansion in these inland cities, layered on top of an already high heat baseline, points toward intensification rather than mitigation of heat risk over the next two decades.

Third, heat warning thresholds should be set locally rather than regionally. The CMA's operational 35 °C threshold treats all stations uniformly, but a 35 °C day in Yancheng (a coastal city averaging 12 to 14 heat days per year) is a substantially more anomalous and physiologically more dangerous event than a 35 °C day in Jinhua (averaging 31 to 36 days per year), where acclimatisation is more developed. Heat-health systems calibrated to relative rather than absolute thresholds, such as the 95th percentile of local daily Tmax used in many European heat-health systems, would provide more equitable protection across the YRD's heterogeneous heat geography.

These three implications share a common premise: that heat adaptation policy should follow the empirical distribution of exposure rather than inherited intuition from megacity-focused literature. I argue this is the most direct and practically actionable contribution of this thesis.

5.6 Limitations

Seven limitations of this study warrant explicit acknowledgement, ordered roughly by severity for the substantive claims advanced above.

First, station-based observational analysis cannot fully separate the contributions of background warming, WPSH variability, and urban heat island development to the observed trends. The Mann-Kendall framework I adopted (§3.4) detects monotonic trend without decomposing it. Wang et al. (2024) showed that near-surface and surface UHI behave differently in the YRD, and a definitive attribution would require integration of surface skin temperature from satellite observations alongside the air temperature data I use here.

Second, the temperature record cannot be cleanly separated from urbanisation-driven warming at the station scale. Several of the 26 stations were originally located in peri-urban environments and have, over the 2000–2024 period, become surrounded by expanding built-up area. Cao et al. (2016) demonstrated that even after formal homogenisation, residual urbanisation contamination of long Chinese temperature records is non-negligible. The ERA5-Land cross-validation I describe in §3.2.1 filters out step changes inconsistent with the reanalysis signal but cannot remove the slower, gradual urbanisation drift that affects the trend estimate.

Third, this study uses only daily maximum temperature exceedance and annual mean temperature. It does not employ the broader ETCCDI suite of indices (Alexander et al., 2006), which includes tropical nights (TR, daily Tmin > 25 °C), warm spell duration (WSDI), and the warmest single-day annual extreme (TXx). Zheng et al. (2021) found that warm night indices have intensified faster than warm day indices in the Chinese northern subtropical zone, suggesting that this study may understate the full picture of heat extreme intensification in the YRD by ignoring the nocturnal component.

Fourth, the socioeconomic data conclude in 2023 while the meteorological data extend to 2024, producing a one-year offset in the correlation analyses. This is unlikely to alter the qualitative conclusions of §4.4, but it does mean that the most recent climate signal is excluded from the socioeconomic comparison.

Fifth, the sample size of n = 26 cities is modest for some of the statistical tests undertaken. Spearman rank correlation with n = 26 has reasonable power to detect ρ ≈ ±0.5 at α = 0.05, but inferences about smaller effects (the panel first-difference coefficients near zero, for instance) carry wider confidence intervals than the point estimates alone suggest.

Sixth, the IDW interpolation reported in §4.2 cannot represent elevation-driven temperature lapse rates in the hilly terrain of southwestern Zhejiang and southern Anhui. Interpolated values in those areas should be treated as approximations rather than as precise estimates, a point I noted in §3.5.

Seventh, this study does not link heat day frequency to health outcomes such as heat-related mortality, hospitalisation, or productivity losses. Without that linkage, claims about which cities are 'most vulnerable' rest on exposure metrics alone, ignoring sensitivity (demographic composition, air conditioning access, building stock thermal performance) and adaptive capacity (warning system coverage, cooling centre availability). I address this gap in §5.7 below.

These seven limitations do not in my judgement undermine the four findings of Chapter 4, but they do constrain the strength of the inferences that can be drawn from them, particularly the inferences about mechanism and attribution that I have explored in §5.2 and §5.4.

5.7 Future Research Directions

Four research directions follow most directly from this study.

The first is multi-source observational integration. The station-based dataset used here would benefit from supplementation with MODIS-derived land surface temperature, ERA5 reanalysis at 9 km resolution, and where available, micrometeorological stations established within urban canopies. Combining these sources would allow direct decomposition of the surface, canopy, and boundary-layer components of YRD heat, and would support the WPSH-versus-urbanisation attribution that station data alone cannot deliver.

The second is the extension to nocturnal indices. Adding tropical nights (TR), warm night frequency (TN90p), and the diurnal temperature range (DTR) to the heat day count used in this study would produce a fuller picture of heat exposure,

particularly relevant for human health outcomes. The asymmetric warming of nights versus days documented by Zheng et al. (2021) at the national scale is likely operating in the YRD as well, and quantifying its specific spatial structure would refine the adaptation-targeting argument advanced in §5.5.

The third is the linkage to health outcomes. The Chinese Disease Surveillance Point system records mortality data at the prefectural level, and several recent studies have linked heat exposure to cardiovascular, cerebrovascular, and respiratory mortality in Chinese cities (Ebi et al., 2021; Zhou et al., 2022). A natural follow-up to this thesis would integrate the 26-city heat day series with mortality records to estimate temperature-mortality functions specific to the YRD's spatial heterogeneity, and to translate the heat day trends quantified here into projected mortality burdens under continued warming.

The fourth is the projection of YRD heat exposure under coupled climate and urbanisation scenarios. CMIP6 downscaled outputs for the 2030s, 2050s, and 2080s, combined with built-up area projections from the YRD urban agglomeration's continued development trajectory, would allow scenario-based analysis of how the present heat geography will evolve. If the maritime moderation mechanism described in §5.3 weakens as sea surface temperatures rise, the inland–coastal heat differential may compress in ways that change which cities are most at risk over the coming decades.

I close this discussion with a brief return to the broader argument of the thesis. The four findings of Chapter 4, interpreted through the literature reviewed in Chapter 2 and the analytical decisions justified in Chapter 3, point to a YRD heat regime that has intensified substantially since 2000, that exhibits a stable inland–coastal geography opposite to the economic-development gradient, and that cannot be productively analysed for urbanisation–heat causation through naive cross-sectional comparison. The most generalisable claim I advance is methodological: regional comparative studies of heat–urbanisation relationships must be conducted with explicit attention to the geographic confound, lest they recover the wrong sign on the very effect they aim to measure. The most policy-actionable claim is spatial: inland secondary cities, not the coastal megaregion, are the priority for heat adaptation in the YRD.

Chapter 6: Conclusion

This thesis has examined the spatiotemporal evolution of extreme heat events across the 26 cities of the Yangtze River Delta urban agglomeration from 2000 to 2024, and the relationship between heat day frequency and three socioeconomic indicators of urban development. Chapter 1 set out the three research questions, Chapter 2 reviewed the literature on which they rest, Chapter 3 documented the data and methods used to address them, Chapter 4 reported the empirical findings, and Chapter 5 interpreted those findings in the context of the literature and the limits of what station-based analysis can establish. This concluding chapter returns to the research questions, summarises what has and has not been answered, identifies the contributions the thesis makes, and signals the broader implications for heat exposure analysis in densely urbanised coastal megaregions.

6.1 Returning to the Research Questions

The three research questions defined in §1.3 admit clear answers from the analyses reported in Chapter 4.

RQ1 asked about the temporal trends and spatial distribution patterns of mean annual temperature and annual heat day frequency across the 26 YRD cities, and about the timing of any structural change in the regional trend. The analyses in §4.1 establish that both variables increased significantly across the period, with regional Sen's slopes of 0.321 days per year for heat day frequency and 0.036 °C per year for mean annual temperature. The sequential Mann-Kendall procedure located a probable mutation point near 2010–2011, after which both variables entered a higher mean state. I have argued in Chapter 5 that no single mechanism among the three plausible candidates (WPSH regime shift, urbanisation-driven local amplification, and accelerated global forcing) can be isolated from station data alone, but that the timing and magnitude of the break are well-established.

RQ2 asked how city-level trend magnitudes vary across the inland–coastal gradient. The city-level Mann-Kendall and Sen's slope analyses in §4.3 show that 12 of the 26 cities have statistically significant upward trends in heat day frequency, with the steepest accumulation rates in inland Zhejiang (Jinhua, $\beta = 0.588$ days yr^{-1}) and inland Anhui (Chuzhou, $\beta = 0.531$; Anqing, $\beta = 0.461$). Coastal cities, while also

warming, accumulate heat days at slower rates. The spatial interpolation reported in §4.2 confirms that this inland–coastal pattern is stable across all four snapshot years, indicating a persistent geographic structure rather than a transient anomaly.

RQ3 asked about the direction and magnitude of the Spearman rank correlation between heat day frequency and each of three socioeconomic indicators, and about the comparison between cross-sectional and within-city panel associations. The analyses in §4.4 report cross-sectional Spearman coefficients of $\rho = -0.572$ for built-up area, $\rho = -0.520$ for permanent resident population, and $\rho = -0.585$ for per capita GDP, all statistically significant at $p < 0.01$ and all in the direction opposite to what the urbanisation-centric literature would predict. The panel first-difference coefficients across the same data are 0.028, 0.044, and 0.007, all near zero and non-significant. I have argued in §5.4 that the cross-sectional negative correlations are an artefact of the geographic confound between coastal position and economic development, that this artefact is predictable given the structure of the YRD dataset, and that the methodological lesson generalises beyond the YRD to any coastal–inland megaregion in which the socioeconomic gradient runs counter to the climatic gradient.

The three research questions are therefore answered, with the appropriate caveats about mechanism attribution that station-based analysis warrants.

6.2 Contributions

The thesis makes three contributions, distributed across the empirical, methodological, and practical registers identified in §1.6.

The empirical contribution is the assembly of a station-observed heat day frequency dataset for all 26 cities of the State Council 2016 YRD boundary across 2000–2024, integrated with a city-level socioeconomic panel for 2000–2023. The temporal extent, spatial coverage, and integration of the two data streams together constitute, to my reading of the literature, the most complete city-scale record of YRD heat exposure assembled to date. The four headline findings derived from this dataset (regional Sen's slope of 0.321 days per year, structural break near 2010–2011, persistent inland–coastal spatial inversion, and the geographic confound in cross-

sectional socioeconomic correlations) provide an empirical baseline against which future YRD heat-exposure assessments can be calibrated.

The methodological contribution is the demonstration that cross-sectional and panel first-difference designs applied to the same dataset can yield qualitatively opposite-looking conclusions, and that the resolution lies in identifying which design holds the relevant confounders constant. I argue this is the thesis's most generalisable contribution. The result is not specific to the YRD: it applies to any megaregion in which the urbanisation gradient is structurally aligned with a climatic gradient, including the Pearl River Delta, the Tokyo–Yokohama–Osaka corridor in Japan, and the US northeastern megalopolis. Researchers undertaking comparable comparative analyses in those settings should expect to obtain similar negative cross-sectional correlations from naive Spearman, and should treat that result as a diagnostic for confounding rather than as evidence about the underlying urbanisation–heat relationship.

The practical contribution is the identification of inland secondary cities, principally those in the Anhui corridor (Chuzhou, Anqing, Xuancheng) and inland Zhejiang (Jinhua, Huzhou), as the cities with the highest absolute heat exposure and the steepest accumulation rates. Adaptation policy in the YRD has, as I noted in §5.5, inherited an attentional bias toward the coastal megacities that dominate economic and political discourse. The data argue for a reallocation of attention toward inland secondary cities. The specific cities I have identified are not at the margins of the YRD plan; they are core cities within the State Council 2016 boundary, with rapidly expanding built-up areas and the highest absolute heat day counts. They are also the cities for which adaptation funding, heat-health warning system coverage, and infrastructural cooling investment have historically lagged the coastal core.

6.3 Limits of the Present Study

I have identified seven specific limitations in §5.6, and rather than repeating them here I want to emphasise the two that most constrain the inferences that can be drawn from the thesis.

The first is the inability of station-based analysis to decompose the observed warming into contributions from background global forcing, WPSH variability, and

urbanisation-driven local amplification. The Mann-Kendall framework I adopted (§3.4) detects monotonic trend without identifying its sources. Where the contributions of the three candidate mechanisms can be separately quantified, future analyses will be able to address attribution questions that this thesis cannot. The structural break analysis in §5.2 documents the existence and timing of a regime change without claiming to explain it.

The second is the absence of nocturnal indices and surface skin temperature measures from the analysis. The heat day count used throughout is a daily maximum temperature exceedance metric. It does not capture the asymmetric warming of minimum temperatures documented by Zheng et al. (2021), and it does not register the surface UHI signal that satellite-derived land surface temperature would. A full picture of YRD heat exposure requires complementary analyses using these alternative measures, which I have identified in §5.7 as a priority direction for follow-up research.

These limitations do not undermine the four findings of Chapter 4, but they do bound the scope of the interpretive claims that can be advanced. The thesis is a station-based observational study, with the strengths and limits that such studies share.

6.4 Broader Implications

I close with two broader implications that follow from the thesis but extend beyond its immediate empirical scope.

The first concerns the relationship between economic geography and climate exposure in coastal megaregions globally. The YRD finding that coastal location moderates heat exposure even as it concentrates economic development is not unique to the YRD. Equivalent patterns are likely operating in any megaregion where the coastal economic core benefits from maritime moderation of summer maximum temperatures, while inland cities lacking that moderation bear higher absolute heat burdens. The structural similarity of the Pearl River Delta, the Greater Tokyo region, and the US northeastern megalopolis to the YRD in this respect suggests that the inversion of heat geography relative to economic geography may be a general feature of coastal megaregion climate, rather than a YRD-specific quirk. Empirical

confirmation in those other settings would be valuable, both for the comparative regional climate literature and for the adaptation-planning communities in those regions.

The second concerns the relationship between cross-sectional and panel designs in environmental social science more broadly. The geographic confound documented in this thesis is one instance of a broader class of confounding problems that arise whenever a putative cause varies spatially in ways that are correlated with other determinants of the outcome. The corrective is not statistical sophistication applied to the cross-sectional data, but a structural shift to a within-unit panel design that holds the confounder constant by construction. This argument has parallels in the broader econometric and epidemiological literatures on confounding by spatial covariates, and the YRD heat analysis offers a concrete worked example of how the corrective operates in practice. I hope the example may be useful to researchers facing analogous problems in other regional contexts.

The two implications share a structural feature. Both point toward the necessity of designs that respect the geography of the phenomenon under study rather than treating spatial heterogeneity as statistical noise. The YRD's heat geography is the product of specific physical and historical conditions, and recovering valid inferences about urbanisation–heat relationships in this region requires methods that hold those conditions constant rather than averaging across them. This is a methodological commitment as much as a substantive finding, and it is the commitment I would carry forward into any subsequent research on heat exposure in densely urbanised coastal regions.

References

Alexander, L. V., Zhang, X., Peterson, T. C., Caesar, J., Gleason, B., Klein Tank, A. M. G., ... & Tagipour, A. (2006). Global observed changes in daily climate extremes of temperature and precipitation. Journal of Geophysical Research: Atmospheres, 111(D5), D05109. https://doi.org/10.1029/2005JD006290

Cao, L., Zhu, Y., Fraedrich, K., & Zhai, P. (2016). Homogenization of daily air temperature dataset in China over 1951–2012. Journal of Climate, 29(13), 4847–4866. https://doi.org/10.1175/JCLI-D-15-0501.1

China Meteorological Administration. (2017). *Meteorological service standard for high-temperature weather* (QX/T 228-2014). China Meteorological Press.

Dietz, T., & Rosa, E. A. (1994). Rethinking the environmental impacts of population, affluence and technology. Human Ecology Review, 1(1), 277–300.

Ding, T., Qian, W., & Yan, Z. (2010). Changes in hot days and heat waves in China during 1961–2007. *International Journal of Climatology*, 30(10), 1452–1462. https://doi.org/10.1002/joc.1989

Ebi, K. L., Capon, A., Berry, P., Broderick, C., de Dear, R., Enright, P., ... & Jay, O. (2021). Hot weather and heat extremes: health risks. The Lancet, 398(10301), 698–708. https://doi.org/10.1016/S0140-6736(21)01208-3

Hao, L., Huang, X., Qin, M., Liu, Y., Li, W., & Sun, G. (2018). Ecohydrological processes explain urban dry island effects in a wet region, southern China. *Water Resources Research*, 54(9), 6757–6771. https://doi.org/10.1029/2018WR023002

Howard, L. (1833). The Climate of London, Deduced from Meteorological Observations. Harvey and Darton.

Huang, Q., & Lu, Y. (2015). The effect of urban heat island on climate warming in the Yangtze River Delta urban agglomeration in China. *International Journal of Environmental Research and Public Health*, 12(8), 8773–8789. https://doi.org/10.3390/ijerph120808773

Kendall, M. G. (1975). *Rank Correlation Methods* (4th ed.). Griffin.

Klein, T., & Anderegg, W. R. L. (2021). A vast increase in heat exposure in the 21st century is driven by global warming and urban population growth. *Sustainable Cities and Society*, 73, 103098. https://doi.org/10.1016/j.scs.2021.103098

Li, H., Shi, L., Jin, X., Tang, X., & Chen, F. (2024). Analysis of land surface temperature drivers and marginal effect on the Yangtze River Delta urban agglomeration using XGBoost-SHAP. *Land*, 13(11), 1951. https://doi.org/10.3390/land13111951

Liu, Y., Peng, J., Sun, J., & Li, X. (2021). Spatiotemporal heterogeneity of Yangtze River Delta urban agglomeration using nighttime light imagery. Remote Sensing, 13(7), 1235. https://doi.org/10.3390/rs13071235

Lu, G. Y., & Wong, D. W. (2008). An adaptive inverse-distance weighting spatial interpolation technique. Computers and Geosciences, 34(9), 1044–1055. https://doi.org/10.1016/j.cageo.2007.07.010

Luo, X., Wei, X., & Chen, J. (2022). Economic drivers of the urban heat island effect in the Yangtze River Delta. Frontiers in Marine Science, 9, 877301. https://doi.org/10.3389/fmars.2022.877301

Mann, H. B. (1945). Nonparametric tests against trend. *Econometrica*, 13(3), 245–259. https://doi.org/10.2307/1907187

National Bureau of Statistics of China. (2024). China City Statistical Yearbook 2023. China Statistics Press.

Oke, T. R. (1982). The energetic basis of the urban heat island. *Quarterly Journal of the Royal Meteorological Society*, 108(455), 1–24. https://doi.org/10.1002/qj.49710845502

Oleson, K. W., Monaghan, A., Wilhelmi, O., Barlage, M., Brunsell, N., Feddema, J., & Hu, L. (2015). Interactions between urbanization, heat stress, and climate change. Climatic Change, 129(3–4), 525–541. https://doi.org/10.1007/s10584-013-0936-8

Peng, S., Piao, S., Ciais, P., Friedlingstein, P., Ottle, C., Breon, F.-M., ... & Myneni, R. B. (2012). Surface urban heat island across 419 global big cities. *Environmental Science & Technology*, 46(2), 696–703. https://doi.org/10.1021/es2030438

Sen, P. K. (1968). Estimates of the regression coefficient based on Kendall's tau. *Journal of the American Statistical Association*, 63(324), 1379–1389. https://doi.org/10.1080/01621459.1968.10480934

Shepard, D. (1968). A two-dimensional interpolation function for irregularly-spaced data. *Proceedings of the 1968 ACM National Conference*, 517–524. https://doi.org/10.1145/800186.810616

Sneyers, R. (1990). *On the Statistical Analysis of Series of Observations* (WMO Technical Note No. 143). World Meteorological Organization.

Spearman, C. (1904). The proof and measurement of association between two things. *The American Journal of Psychology*, 15(1), 72–101. https://doi.org/10.2307/1412159

State Council of China. (2016). *Yangtze River Delta Urban Agglomeration Development Plan*. General Office of the State Council.

Wang, M., He, G., Zhang, Z., Wang, G., Zhang, Z., Cao, X., ... & Liu, X. (2024). Comparison of near-surface and surface urban heat islands in the Yangtze River Delta. Frontiers in Environmental Science, 12, 1387672. https://doi.org/10.3389/fenvs.2024.1387672

Wang, M., He, G., Zhang, Z., Wang, G., Zhang, Z., Cao, X., & Liu, X. (2024). Comparison of near-surface and surface urban heat islands in the Yangtze River Delta. Frontiers in Environmental Science, 12, 1387672. https://doi.org/10.3389/fenvs.2024.1387672

Xie, M., Liao, J., Wang, T., Zhu, K., Zhuang, B., Han, Y., ... & Li, S. (2017). Modeling the impact of urbanization on the summertime boundary layer heat stress and its implications for heat island effect. Atmospheric Chemistry and Physics, 17(8), 5439–5454. https://doi.org/10.5194/acp-17-5439-2017

Yin, H., & Sun, Y. (2018). Characteristics of extreme temperature and precipitation in China in 2017 based on ETCCDI indices. Advances in Climate Change Research, 9(4), 218–226. https://doi.org/10.1016/j.accre.2019.01.001

York, R., Rosa, E. A., & Dietz, T. (2003). STIRPAT, IPAT and ImPACT: analytic tools for unpacking the driving forces of environmental impacts. Ecological Economics, 46(3), 351–365. https://doi.org/10.1016/S0921-8009(03)00188-5

Zhai, J., Liu, R., Liu, J., Huang, J., & Qin, G. (2020). Influence of the economic efficiency of built-up land on urban heat islands in the Yangtze River Delta urban agglomeration. Remote Sensing, 12(23), 3944. https://doi.org/10.3390/rs12233944

Zheng, Y., Li, J., Feng, S., & Guo, H. (2021). Variations of extreme temperature event indices in six temperature zones in China from 1961 to 2020. *Atmosphere*, 12(11), 1398. https://doi.org/10.3390/atmos12111398

Zhou, B. T., & Qian, J. (2021). Changes of weather and climate extremes in the IPCC AR6. *Climate Change Research*, 17(6), 713–718. https://doi.org/10.12006/j.issn.1673-1719.2021.167

Zhou, L., He, C., Kim, H., Honda, Y., Hashizume, M., Kinney, P. L., ... & Guo, Y. (2022). The burden of heat-related stroke mortality under climate change scenarios in 22 East Asian cities. Environment International, 170, 107602. https://doi.org/10.1016/j.envint.2022.107602

Appendix A: Full City-Level Statistical Tables

Tables A1 and A2 below report the complete Mann-Kendall and Sen's slope statistics for all 26 cities. The compressed versions in Chapter 4 (Tables 4.1 and 4.2) include the columns most directly used in the analytical narrative; the appendix retains the full set for reference.

[Tables A1 and A2 — copy from Results_LIU_YIXIAN_23061733_clean.docx]